



HAL
open science

Development and characterisation of soluble polymeric particles for pulmonary peptide delivery

Frédéric Tewes, Lidia Tajber, Owen I Corrigan, Carsten Ehrhardt,
Anne-Marie Healy

► **To cite this version:**

Frédéric Tewes, Lidia Tajber, Owen I Corrigan, Carsten Ehrhardt, Anne-Marie Healy. Development and characterisation of soluble polymeric particles for pulmonary peptide delivery. *European Journal of Pharmaceutical Sciences*, 2010, 41 (2), pp.337-352. 10.1016/j.ejps.2010.07.001 . inserm-01102826

HAL Id: inserm-01102826

<https://inserm.hal.science/inserm-01102826>

Submitted on 13 Jan 2015

HAL is a multi-disciplinary open access archive for the deposit and dissemination of scientific research documents, whether they are published or not. The documents may come from teaching and research institutions in France or abroad, or from public or private research centers.

L'archive ouverte pluridisciplinaire **HAL**, est destinée au dépôt et à la diffusion de documents scientifiques de niveau recherche, publiés ou non, émanant des établissements d'enseignement et de recherche français ou étrangers, des laboratoires publics ou privés.

Development and characterisation of soluble polymeric particles for pulmonary peptide delivery

Tewes F, Tajber L, Corrigan OI, Ehrhardt C and Healy AM.

Trinity College Dublin, School of Pharmacy and Pharmaceutical Sciences, Dublin 2, Ireland.

Correspondence should be addressed to:

Dr. Anne Marie Healy, School of Pharmacy and Pharmaceutical Sciences, University of Dublin,

Trinity College, Dublin 2, Ireland, Tel.: +353-1-896-1444; fax +353-1-896-2783, e-mail:

healyam@tcd.ie

Abstract

Pulmonary administration of protein and peptide drugs using inhaled dry powder particles is an interesting alternative to parenteral delivery. The stabilisation of these molecules is essential to the maintenance of biological activity in such inhalation formulations. Here salmon calcitonin (sCT) was co-spray dried with linear or branched PEG (L-PEG and B-PEG) and PVP in order to formulate aerosolisable particles of the bioactive peptide. Co-spray drying L-PEG and PVP resulted in porous particles, with minimal D_{50} (median volume diameter) and MMAD (mass median aerodynamic diameter) values obtained for a PEG/PVP w/w ratio of 1. For particles based on both L-PEG and B-PEG, an increase in acetone, a poor solvent for the PVP, up to 70 wt% of the spray dried solution led to a decrease in D_{50} and MMAD. Crystallinity of PEG in the particles ranged between 90-97% when the PVP content varied between 15 and 70 wt%, indicating a low degree of interaction between PVP and PEG. Additionally, dynamic vapour sorption analysis showed that an increase in PVP content increased the particle surface hygroscopicity. Hence, particle properties were adjusted by altering the water/acetone and PEG/PVP ratio in the spray dried solutions. PVP present at the particles surface protects them from melting during the spray drying process but also increases their hygroscopicity, adversely affecting their aerodynamic properties. Targeting a 5 wt% of sCT loading resulted in a loading efficiency of 77.9% and 83.6% with L-PEG and B-PEG based particles, respectively. Loading of sCT in L-PEG or B-PEG based particles modified particle roughness and D_{50} , leading to an increase in MMAD of the L-PEG based particles. However, particles were still considered to be suitable for aerosolisation as their FPFs (fine particle fractions) were higher than 30%. These particles formulated with PVP and PEG allowed sCT biological activity to be maintained when evaluated by measuring cAMP production by T47D cells.

Keywords: Pulmonary inhalation, microparticles, peptide, spray drying, PEG.

Introduction

Due to the advances in biotechnology many peptide and protein drugs have been developed that, in most cases, can be delivered only by parenteral injection. This route of administration, however, often leads to low patient compliance and requires qualified personnel. Hence, new non-invasive delivery strategies for these bioactives have been extensively explored. Among these, inhalation delivery has proven to be especially attractive, due to the high lung epithelium surface area and good lung vascularisation resulting in fast absorption from this organ (Cheng and Lim, 2009, Kompella and Lee, 2001, Patton, 1998, Youn *et al.*, 2008). A few inhalable peptide formulations have already been marketed such as PulmozymeTM or ExuberaTM, although the latter has been withdrawn from the market mainly due to patients' dissatisfaction linked to the complexity of the inhaler device used (Mitri and Pittas, 2009). Hence, while promising, systemic inhalation therapy is not yet optimised. Furthermore, most existing aerosol systems are not designed to protect delicate macromolecules such as proteins.

To have a systemic effect, inhaled particles are believed to need to reach the alveoli and in order to do so they must possess a narrow aerodynamic particle size distribution. In fact, numerous experimental and theoretical studies have demonstrated that particles with a median aerodynamic diameter of 1–5 μm deposit maximally in the distal lung (Edwards and Dunbar, 2002).

Among the factors that can be adjusted to optimise the efficiency of aerosol formulations, particle chemistry and surface morphology, manipulated to reduce particle-particle interactions and hygroscopicity, are well documented (Chow *et al.*, 2007, Healy *et al.*, 2008). Polyethylene glycol (PEG) polymers are materials that could be used to engineer the particle surface to reduce particle-particle interactions and improve their aerodynamic properties. Moreover, PEG polymers adsorbed or grafted to the particle surface with a special conformation have been used

to reduce particle clearance by phagocytosis. Additionally, many formulation processes are too stressful for fragile protein/peptide APIs, leading to a potential loss of their activity. In this context PEGs can be used to protect or stabilise proteins from unfolding and activity loss during and after the formulation process (Pean *et al.*, 1999). A number of studies have used PEGs covalently bound to proteins to stabilise them and increase their half-life *in vivo* (Filpula and Zhao, 2008, Youn *et al.*, 2008). PEGs have also been investigated as carriers for dry powder inhalers (DPI) (Corrigan *et al.*, 2004). PEG 6 kDa was capable of improving the *in vitro* deposition of bovine serum albumin using a Rotahaler[®] (Lucas *et al.*, 1998). Additionally, PEGs with molecular weights (M_w) ranging from 400 Da to 10 kDa were administered to animals by the intravenous route in numerous studies without noticeable toxic effects (Bailon and Berthold, 1998, Vicent and Duncan, 2006).

Spray drying is a process of choice to obtain particles with a narrow size distribution, (Chan *et al.*, 2004, Chow *et al.*, 2007, Seville *et al.*, 2007). Furthermore, this process allows porous microparticles to be formulated, which are known to be beneficial for drug delivery to the respiratory tract by oral inhalation as they have reduced interparticulate attractive forces and improved flow characteristics relative to nonporous micronised drug materials (Healy *et al.*, 2008, Nolan *et al.*, 2009). These particles have potential for improved efficiency of administration to the lungs in the dry form using a DPI. However, because of their low melting temperature ($T_m \sim 60^\circ\text{C}$), it is difficult to spray dry PEG polymers with the most frequently used solvents, such as water or ethanol, as the outlet temperature in the spray dryer is too close to their T_m , leading to fused, aggregated material (Corrigan *et al.*, 2002). A possible solution to overcome this problem is the use of another excipient, with a high T_m or a high glass transition temperature (T_g), which is able to protect the particle surfaces from fusing. In terms of available

biocompatible materials, polyvinylpyrrolidone (PVP) polymers appear to be potential candidates to stabilise protein/peptide loaded PEG particles. In fact, they have a T_g ranging from 95°C to 175°C depending on the M_w (Haaf *et al.*, 1984), have previously been used in spray drying processes and have been used to protect or stabilise protein during formulation (D'Souza *et al.*, 2004, Reddy *et al.*, 2009, Yoshioka *et al.*, 2006).

In the present paper, we describe a process for formulating peptide-loaded microparticles made of soluble polymer and designed for pulmonary delivery. Salmon calcitonin (sCT), a model peptide, was mixed with a linear PEG (L-PEG) or branched PEG (B-PEG) along with PVP and co-spray dried to formulate microparticles. Polymers with a molecular weight of 10 kDa were used to ensure their diffusion from the lung parenchyma into the blood circulation and then their renal clearance, as it is known that the glomerulus cut off for these polymers is around 30 kDa (Haaf *et al.*, 1984). Micromeritic, thermal and aerodynamic properties characterisation studies of the prepared microparticles are presented. sCT-loaded particles were also evaluated in terms of loading and biological activity.

1. Materials and methods.

1.1. Materials.

L-PEG 10kDa (L-PEG) and PVP 10kDa (K15) were purchased from Fluka (Munich, Germany). Four-armed branched PEG 10kDa (B-PEG) was purchased from JenKem Technology USA Inc (Allen, USA). Salmon calcitonin acetate salt (sCT) was purchased from Polypeptide Laboratories (Malmö, Sweden). XRD and DSC experiments showed that sCT raw material was amorphous (data not shown). Deionised water was produced by a Purite Prestige Analyst HP water purification system (Millipore, Carrigtwohill, Ireland). HPLC grade acetonitrile was purchased from Sigma-Aldrich (Dublin, Ireland). Other chemicals were of analytical grade and purchased from Sigma-Aldrich.

1.2. Methods.

1.2.1. Spray Drying.

PEG (linear or branched) and PVP were spray dried as solutions having a total polymer concentration of 1% w/w using a Büchi B-290 Mini spray dryer (Büchi, Flawil, Switzerland) set in the closed cycle mode with a 2-fluid nozzle. Solutions were composed of acetone/water mixtures varying in weight proportion ranging from 50/50 to 85/15. PVP/PEG weight ratio varied from 15/85 to 70/30. Experimental conditions were as follows: inlet temperature was fixed at 65°C; feeding pump was set at 30% (8 mL/min). Spraying nitrogen nozzle flow rate was 15 L/min. Nitrogen flowing at 630 L/min was used as the drying gas (aspirator rate 100%). Those conditions resulted in an outlet temperature ranging from 36 to 41°C. Preliminary experiments showed that a total polymer concentration of 1% w/w was optimal for spray drying. An increase in polymer concentration produced large and dense particles, not suitable for pulmonary administration.

1.2.2. Thermogravimetric Analysis (TGA).

TGA was performed using a Mettler TG 50 (Mettler Toledo Ltd., Greifensee, Switzerland) linked to a Mettler MT5 balance having 0.0001 mg of readability. Data was processed using Mettler Toledo STAR^e software. Accurately weighed samples (approx. 10 mg) were analysed using open pans under nitrogen purge. Samples were run at a heating rate of 10°C/min from 25 – 200°C.

1.2.3. Differential Scanning Calorimetry (DSC).

DSC was performed using closed 40 µL-aluminium pans with three vent holes on samples (4 – 8 mg) weighed with a MT5 balance. Samples were run at a heating rate of 10°C/min under nitrogen purge from –50°C to 200°C using a Mettler Toledo DSC 821^e. Mettler Toledo STAR^e software was used for analysis of thermal events. Relative degree of crystallinity of PEG polymer in the PVP-PEG mixture systems was calculated (Eq. (1)) using the melting enthalpy of the PEG raw material ($\Delta H_{f,PEG}$), melting enthalpy of the PEG in the polymer systems ($\Delta H_{f,PEG \text{ in BLEND}}$) and the percentage of weight of PEG (wt%) in the blend, as previously described (Janssens *et al.*, 2008):

$$\text{Crystallinity(\%)} = \frac{\Delta H_{f,PEG \text{ in BLEND}}}{\Delta H_{f,PEG} \times \text{wt\%}} \times 100 \quad (1)$$

1.2.4. Scanning Electron Microscopy (SEM).

Scanning electron micrographs of powder samples were taken using a Hitachi S-4300N (Hitachi Scientific Instruments Ltd., Tokyo, Japan) or a Tescan Mira XMU (Brno, Czech Republic) scanning electron microscope. The dry powder samples were fixed on aluminium stubs with double-sided adhesive tape and a 10 nm-thick gold film was sputter coated on the samples before visualisation. Primary electrons were accelerated under a voltage of 5 kV. Images were formed from the collection of secondary electrons.

1.2.5. Powder X- ray Diffraction (XRD).

X-ray powder diffraction measurements were conducted on samples placed in a low background silicon holder, using a Rigaku Miniflex II desktop X-ray diffractometer (Rigaku, Tokyo, Japan) with Bragg-Brentano geometry. The samples were scanned over a range of $5 - 40^\circ 2\theta$ at a step size of 0.05° per second. The X-ray tube composed of Cu anode was operated under a voltage of 30 kV and a current of 15 mA, which, after crossing a monochromator, produced Cu $K\alpha$ radiation ($\lambda = 1.542 \text{ \AA}$). A scintillation detector detected the X-rays after crossing a $K\beta$ filter.

1.2.6. Particle size distribution analysis.

The particle size distributions were determined by laser diffraction using a Malvern Mastersizer 2000 (Malvern Instruments Ltd. Worcestershire, UK) with the Scirocco 2000 dry powder feeder to disperse the particles. Samples were run at a vibration feed rate of 50% and the dispersive air pressure used was 2 bar. Refractive indices were 1.455 (true part) and 0.01 (imaginary part) for the particles and 1.0 for the air. Data were analysed based on the equivalent volume median diameter D_{50} and the span of the particle size volume distribution. The particle size distribution of each sample was determined in triplicate.

1.2.7. Dynamic Vapour Sorption (DVS).

Vapour sorption experiments were performed on a DVS Advantage-1 automated gravimetric vapour sorption analyzer (Surface Measurement Systems Ltd., London, UK). The DVS-1 measures the uptake and loss of vapour gravimetrically with a mass resolution of $\pm 0.1 \mu\text{g}$. The temperature was maintained constant at $25.0 \pm 0.1^\circ\text{C}$. Around 10 mg of powder was loaded into a sample net basket and placed in the system. The samples were equilibrated at 0% of relative humidity (RH) to remove any surface water present and establish a dry reference mass. The samples were then exposed to the following % of RH profile: 0 to 90% in 10% steps and the

same for desorption. At each stage, the sample mass was allowed to reach equilibrium ($dm/dt \leq 0.002$ mg/min for 10 min) before the partial pressure was increased or decreased. An isotherm was calculated from the complete sorption and desorption profile. The amount of water was expressed as a percentage of the dry sample. The Young–Nelson equations were used as previously described (Alvarez-Lorenzo *et al.*, 2000) to fit experimental equilibrium sorption and desorption data of the isotherms:

$$M_s = A(\beta + \theta) + B\theta RH \quad (2)$$

$$M_d = A(\beta + \theta) + B\theta RH_{\max} \quad (3)$$

where M_s and M_d are, respectively, the mass percentage of water contents of the polymer system at the equilibrium for each %RH during sorption and desorption. A and B are constants characteristic of each system. In this model, θ is the fraction of the surface covered by at least one layer of water molecules. It is defined as follows, with E a constant depending of the material.

$$\theta = RH/(RH + E(1 - RH)) \quad (4)$$

And β is defined by the following equation:

$$\beta = -E \times RH / (E - RH \times (E - 1)) + E^2 / (E - 1) \times \ln[E - RH(E - 1) / E] - (E + 1) \times \ln(1 - RH) \quad (5)$$

Thus, $A\theta$ is the mass of water in a complete adsorbed monolayer expressed as a percentage of the dry mass of the sample. $A(\beta + \theta)$ is the total amount of adsorbed water, and $A\beta$ is the mass of water which is adsorbed beyond the mass of the monolayer (i.e., in multilayer or cluster adsorption). B is the mass of absorbed water at 100% of RH, and, hence, $B\theta RH$ is the mass of absorbed water when the water coverage is θ for a given %RH. The experimental data were fitted using Eq. (2) and (3) by means of an iterative multiple linear regression using, as fitting

criteria, the sum of the squares of the residuals between the experimental and the calculated values. The degree of adjustment was expressed by the multiple correlation coefficient (Microsoft Excel 2003). According to the model characteristics, from the estimated values of A , B , and E , the corresponding profiles of water adsorbed in monolayer ($A\theta$), multilayer ($A\beta$) and absorbed water ($B\theta RH$) were obtained.

1.2.8. Aerodynamic particle size analysis.

The aerodynamic particle size distribution was measured using a Next Generation Impactor (NGI, Copley Scientific Limited, Nottingham, UK) operated under pharmacopoeial conditions (2009). The flow rate was adjusted to get a pressure drop of 4 kPa in the powder inhaler (Handihaler[®], Boeringher Ingelheim, Ingelheim, Germany) and the time of aspiration was adjusted to obtain 4 L, typical for inspiration by a patient. The dry powder inhaler was loaded with a no. 3 hard gelatin capsule loaded with 20 ± 2 mg of powder for each test. After dissolution in an appropriate volume of water, particle deposition in the device, the throat and all the stages and the filter was determined by the chromatographic analysis further described in section 2.2.10. For accuracy, each test was repeated three times. The total amount of particles with aerodynamic diameters smaller than $5.0 \mu\text{m}$ was calculated by interpolation from the inverse of the standard normal cumulative mass distribution less than stated size cut-off against the natural logarithm of the cut-off diameter of the respective stages. This amount was considered as the fine particle fraction (FPF) and expressed as a percentage of the emitted recovered dose (ED). The mass median aerodynamic diameter (MMAD) of the particles was defined from the same plot as the particle size at which the line crosses the 50% mark.

1.2.9. sCT loaded particles

The quantity of sCT encapsulated in the particles was determined by dissolving a known amount of particles (around 10 mg) in a volumetric flask and then assaying the sCT concentration by the HPLC method described below. The loading was defined as the mass of sCT divided by the mass of particles. The loading efficiency was defined as the ratio between the theoretical and experimentally determined loading.

1.2.10. Chromatographic analysis

- PVP assay

In order to determine the amount of particles deposited in the different stages of the NGI, a PVP assay performed by separation by size exclusion chromatography (SEC) with a PL aquagel-OH 30, 8 μm , 300 x 7.5 mm column (Polymer Laboratories, Shropshire, UK) and UV absorbance detection was set up. The SEC measurements were conducted by injecting 200 μL in the LC module I plus chromatography System (Waters, City, UK) composed of a pump, an autosampler and a spectrophotometer set up for measuring absorbance at 215 nm. Pure water, running at a flow rate of 1.5 mL/min, was used as the mobile phase. Standard solutions were prepared by mixing equal amounts of PVP and PEG to take into account the influence of the latter on the assay. The PVP concentration ranged from 0.5 to 0.0125 mg/mL. Chromatograms were composed of two peaks corresponding to different distributions of M_w present in the commercial PVP K15. Calibration curves were prepared by using the areas of the two peaks. Calibration curves and three levels of controls (low, middle and high) were performed for every set of measurement. Assays were validated if bias on the controls were lower than 15% and the coefficient of determination (r^2) of the calibration curve higher than 0.99. Between-run precision

and accuracy, calculated by measuring the CV and bias of the controls using 5 different calibration curves, respectively, were both, for the three controls point values, lower than 5%.

- sCT assay

sCT HPLC assay was performed using the same LC module I plus (Waters, UK) chromatographic system set up with a C18, 15-20 μm , 3.9 x 300 mm apolar column ($\mu\text{Bondapak}^{\text{TM}}$, Waters). Measurements were conducted by injecting 50 μL of samples, standards or controls in the mobile phase running at 1.5 mL/min and composed of 64% in volume of aqueous phase (1.8 g/L of NaCl, 0.05% v/v of TFA dissolved in H_2O) and 36% of acetonitrile. sCT was detected by measuring the absorbance at 214 nm. Standards for the calibration curves were prepared by mixing sCT with PVP and PEG in similar proportion to the theoretical loading of the particle, to take into account the influence of the excipients on the assay. sCT concentration of the standards ranged from 0.1 mg/mL to 0.003 mg/mL. Calibration curves and controls were performed for every set of measurements. Assays were validated if bias on the controls were lower than 15% and r^2 of the calibration curve higher than 0.99.

1.2.11. *In vitro* bioactivity.

The capacity of sCT formulations to increase intracellular cAMP was assessed in accordance with a previously reported method (Ryan *et al.*, 2009, Youn *et al.*, 2006, Youn *et al.*, 2008). T47D human breast cancer cells expressing calcitonin receptors were maintained in RPMI 1640 culture medium supplemented with 1% v/v penicillin–streptomycin (Sigma), 10% v/v foetal bovine serum (Sigma), and 0.2 IU/mL insulin (Sigma). Cells were seeded on 24-well plates at an initial density of 1.0×10^6 cells/well and incubated in air with 5% of CO_2 at 37°C for 2 days. After washing with serum free medium, cells were pre-incubated with the fresh medium supplemented with the phosphodiesterase inhibitor, 3-isobutyl-1-methyl-xanthine (IBMX,

200 μ M) at 37°C for 30 min. The cells were then incubated for 15 min with sCT formulations dissolved in serum free RPMI 1640 plus IBMX. After removing the supernatant, the intracellular cAMP was extracted from the cells by cell lysis and measured by ELISA (R&D Systems, Abingdon, UK).

1.2.12. Statistical data analysis

When there were more than two sets of data, they were statistically evaluated by an analysis of variance (ANOVA) test with Bonferroni's multiple comparison tests as post-hoc test. Otherwise, statistical analysis was undertaken using Student *t*-test.

2. Results.

2.1. Blank particles.

2.1.1. Effect of L-PEG/PVP w/w ratio.

Particle morphology.

SEM micrographs of spray dried L-PEG – PVP systems are shown in Figure 1. A decrease in particle fusion can be observed with an increase in PVP content. At low PVP content (15 and 30 wt% of PVP), particles appeared solid, melted and fused (Fig. 1A and 1B). At high PVP concentration (50 and 70 wt% of PVP), particles appeared isolated and spherical (Fig. 1C and 1D). The PVP/L-PEG ratio also influenced the particles' surface morphology. For 15 and 30 wt% of PVP, particle surfaces were smooth, whereas for 50 wt%, their surfaces were rough and presented some convolutions (Fig. 1C'). A further increase in PVP amount to 70 wt% led to the formation of hollow particles with a flat non-porous outside surface, but presenting some pores on the internal surface (Fig. 1D').

Thermogravimetric analysis.

Thermogravimetric analysis measurements performed between 20 °C and 200 °C on particles made with various PVP/PEG weight ratios showed a loss of mass from 20 to 60 °C. A further increase in temperature to 200 °C did not lead to further mass loss. The higher the PVP concentration was, the higher the mass loss. For 15 wt% of PVP, the mass loss was 0.55 wt%, then increased to 1.48 wt% and 4.78 wt% for a PVP concentration of 50 and 70 wt%, respectively.

Dynamic vapour sorption.

The isotherms of water vapour uptake obtained for the L-PEG – PVP systems and individual components are shown in Figure 2. According to the IUPAC classification, the isotherm shape

obtained with L-PEG raw material displayed an adsorption mechanism dominated by type III behaviour, having low moisture uptake for a large range of %RH (0-80%) and then adsorbing most of the water at high %RH. Isotherms obtained with PVP raw material showed an adsorption mechanism dominated by type II behaviour (IUPAC, 1986), adsorbing a large amount of water at low %RH (0-30%) to reach a saturation state and then adsorbing more water at high %RH. For the isotherms obtained with the spray dried L-PEG – PVP systems, an increase in the PVP amount proportionally increased the type II behaviour. In addition to the variation of their shape, some isotherms showed closed hysteresis loops between adsorption and desorption branches at low (see insert in Fig. 2) and at high %RH. Hysteresis can have various causes. For amorphous and semi-crystalline polymers the main reason is bulk absorption of water (Agrawal *et al.*, 2004, Alvarez-Lorenzo *et al.*, 2000, Bravo-Osuna *et al.*, 2005). Thus, the presence and distribution of moisture in various forms has been determined by establishing quantitative correlations between equilibrium moisture content and the %RH using the Young and Nelson theory (Agrawal *et al.*, 2004, Alvarez-Lorenzo *et al.*, 2000, Bravo-Osuna *et al.*, 2005). This theory divides moisture sorption into three basic mechanisms: surface adsorption, solvent condensation (multilayer or cluster) and bulk absorption. It provides equations to fit these contributions separately (Eq. 2 and 3). Fitting DVS data with the Young – Nelson model shows that, for most of the %RH range, the L-PEG raw material adsorbed few water molecules as a monolayer, since the surface coverage, θ , was equal to only 0.13 for a RH of 80%. At 90% of RH, PEG suddenly absorbed a lot of water (29 wt%) and adsorbed 12 wt% as clusters or multilayer. For PEG, absorption represents the main way in which water is taken up, as can be confirmed by the low values of the *A* parameter, compared with those of the *B* parameter of the Young-Nelson equations (Table 1). In contrast, the PVP raw material was almost saturated with

a water monolayer (8.9 wt%) after an exposure at 50% of RH (Fig. 3). After 60% completion of the water monolayer, water molecules were adsorbed as multilayers to reach 35 wt% of the PVP at 90% of RH. In the range of %RH values investigated, PVP linearly absorbed water molecules to reach 6.8 wt% of polymer at 90% of RH. As the proportion of PVP increased in the L-PEG – PVP systems, the *A* parameter of the Young and Nelson equation increased, showing the increase in the capacity of these particles to adsorb water. The *B* parameter increased to reach a maximum value for 50 wt% of PVP in the particles, and then dramatically decreased for 70 wt% of PVP. This result suggested that particles made of 50 wt% of L-PEG have the highest ability to absorb water at high %RH, which could be attributed to the higher porosity of these particles.

Solid state analysis.

The crystallinity of the L-PEG in the PEG–PVP systems was evident from the presence of the two main diffraction Bragg peaks in the diffractograms (Fig. 4A), characteristic of PEG polymers (Corrigan *et al.*, 2004, Janssens *et al.*, 2008). DSC thermograms of L-PEG–PVP systems are presented in Figure 4B. For all the PEG/PVP ratios, thermograms showed only one endothermic peak of melting around 60°C, also illustrating the crystallinity of the L-PEG in the systems. The presence of PVP slightly shifts the peak position from 62.5°C for the pure L-PEG raw material to 59.5°C in the presence of 70% PVP. The relative degree of crystallinity of L-PEG in the polymer systems was calculated using the melting enthalpy of the L-PEG raw material and Equation (1), which takes into account the dilution of the PEG by the PVP (Fig. 4C). The relative degree of crystallinity of L-PEG remained high even when spray dried in the presence of 70 wt% of PVP ($83.9 \pm 5.2\%$). This suggests weak or no interactions between the polymers.

Particle size distribution and aerodynamic properties.

When spray dried from a solution containing 50 wt% of acetone, volumetric particle size distributions of the different L-PEG – PVP systems, measured by laser diffraction, were bimodal with a wide particle size range (data not shown) as described by the span values ranging from 1.7 to 9.0. Median values (D_{50}) of these particle size distributions are shown in Figure 5. The D_{50} decreased significantly as the PVP/PEG weight ratio was increased, reaching a minimum for a 1/1 w/w ratio. A further increase in PVP/PEG weight ratio did not significantly change the median of the particle size distribution. The aerodynamic properties of particles formulated with 50 and 70 wt% of PVP are shown in Figure 5. The MMAD of particles formulated with 50 wt% of PVP (7.3 μm) was significantly lower than for those formulated with 70 wt% of PVP (11.3 μm), whereas the FPFs were similar (~ 22%).

As the particles made of L-PEG and PVP with a weight ratio equal to 1 gave better preliminary results, this ratio was used in the following experiments.

2.1.2. Effect of acetone/water weight ratio.

In order to evaluate the influence of the acetone/water weight ratio in the spray dried solutions, we also formulated particles using 70 or 85 wt% of acetone, all the other parameters being constant. From 85 wt% of acetone the solution became cloudy with a blue hue, which could be attributed to the nanoprecipitation of the PVP. In fact, acetone is a poor solvent for the PVP and can induce this selective precipitation (Haaf *et al.*, 1984, Jirgensons, 1952).

Particle morphology.

SEM micrographs of 1/1 w/w PVP/L-PEG systems spray dried from solutions composed of 70 and 85 wt% of acetone are shown in Figure 6A-B. SEM micrographs showed individual spherical particles with porous rough surfaces, as for particles formulated with 50 wt% of

acetone (Fig. 1C'). However, whereas the particles formulated with 50 wt% of acetone looked filled, particles formulated with 70 wt% looked more hollow and fragile.

Solid state analysis.

The concentration of acetone in the spray dried solution did not influence the crystallinity of L-PEG in the PEG-PVP systems as the area of the two main Bragg peaks (Fig. 7A) and the normalised melting enthalpy of L-PEG (Fig. 7B) remained statistically significantly unchanged when the acetone concentration was changed. The L-PEG relative degree of crystallinity within the polymer blend, calculated using Equation (1) ranged from $87.8 \pm 4.6\%$ to $90.5 \pm 4.7\%$.

Particle size distribution and aerodynamic properties.

Micromeritic and aerodynamic properties of particles spray dried from different water/acetone weight ratios are described in Figure 8. In the presence of 70 and 85 wt% of acetone, the volumetric particle size distributions were monomodal and narrow as suggested by the span ranging from 1.3 to 1.7 (data not shown). However, the D_{50} did not change significantly with the increase in acetone concentration in the spray dried solutions (Fig. 8). Interestingly, the increase in acetone concentration up to 70% led to a significant decrease in the average MMAD in comparison to the values obtained with 50 wt% of acetone. An additional increase up to 85 wt% did not modify the MMAD compared to that obtained with 70 wt%. Similarly, the increase in the acetone concentration up to 70 wt% led to a significant increase in the average FPF, whereas no significant difference was observed for systems spray dried from 85 wt% of acetone.

2.1.3. Four-armed branched PEG (B-PEG).

PEG polymers can be synthesised with different shapes that may have a different impact on the peptide/protein stabilisation (Fee, 2007). With the aim of comparing the influence of the

structure of the PEG on the particle properties, particles made of PVP and B-PEG were formulated.

Particle morphology.

SEM micrographs of PVP–B-PEG particles spray dried from solution containing 1 wt% of polymers having a weight ratio of 1 and made of 50 or 70 wt% of acetone are shown in Figure 6C – 6D. In contrast to particles made of L-PEG (Fig. 6A), SEM micrographs showed that B-PEG–PVP particles formulated from solutions composed of 50 wt% of acetone were fused and had smooth surfaces. Thus, these particles were not considered to be suitable for aerosolisation. However, particles formulated from solutions composed of 70 wt% of acetone were isolated, spherical, hollow and with rough surfaces. These particles have similar morphology to those obtained with L-PEG using 50 to 85 wt% of acetone in the spray dried solutions (Fig. 1C and Fig. 6A-B).

Solid state analysis.

X-ray diffractograms (Fig. 7C) and DSC thermograms (Fig. 7D) of the B-PEG raw material showed that, as for the L-PEG raw material, the polymer was crystalline. The peak temperature of the melting endotherm was 61.7°C (Fig. 7D). This endotherm was characterised by a concave melting curve starting at 44°C. In the presence of 50 wt% of PVP, the peak temperature of the melting endotherm of the B-PEG was shifted to ~53°C. The changes in water/acetone ratio in the spray dried solution did not affect the peak position. The relative degree of crystallinity of B-PEG in the polymer systems, calculated using Equation (1) and $\Delta H_f^{\text{PEG}} = 166 \text{ J/g}$ for the B-PEG raw material, was $87.9 \pm 6.2\%$ and $91.8 \pm 4.6\%$ for particles formulated from solutions containing 50 and 70 wt% of acetone, respectively.

Particle size distribution and aerodynamic properties.

The average D_{50} of the volumetric particle size distribution and aerodynamic properties of particles formulated using B-PEG and different water/acetone ratios are described in Figure 8. When spray dried from a solution containing 50 wt% of acetone, the volumetric particle size distributions were bimodal with an average D_{50} of $7.0 \pm 0.4 \mu\text{m}$. They displayed a wide distribution characterised by an average span of 7.2 ± 0.3 . Increasing the amount of acetone to 70 wt% allowed the production of particles having a monomodal size distribution with an average D_{50} and span values of $4.5 \pm 0.2 \mu\text{m}$ and 1.8 ± 0.2 , respectively. As particles formulated from solution containing 50 wt% of acetone were fused and not uniform in shape, the evaluation of aerodynamic properties was performed on particles produced from solution containing 70 wt% of acetone only. The average MMAD ($6.12 \mu\text{m}$) was higher than the D_{50} of the geometric particle size distribution. Comparing average MMAD and FPF values of particles formulated with B-PEG and L-PEG using Bonferroni's multiple comparison tests as post-hoc test of ANOVA showed that MMAD and FPF of the L-PEG based particle were significantly lower and higher, respectively ($p < 0.05$), than of the B-PEG based particles.

2.2. Salmon calcitonin loaded particles.

In order to evaluate the capacity of the B-PEG and L-PEG polymers based particles to encapsulate and stabilise sCT, two types of sCT-loaded particles using an amount of sCT equal to 5 wt% of the total polymer amount (4.8 wt% of the particle) were formulated. For all these formulations, the spray dried solutions were composed of 70 wt% of acetone and 1 wt% of polymer with a PEG/PVP weight ratio of 1.

Particle morphology.

SEM micrographs of PVP/L-PEG and PVP/B-PEG sCT loaded particles are shown in Figure 6E and 6F, respectively. Both types of particle appeared isolated and spherical. In contrast to the blank (unloaded) particles (Fig. 6A and 6D), the surface of the loaded particles looked much less nanoporous. However, sCT-loaded particles made of L-PEG were still hollow. Whereas the morphology of both blank particles, linear and branched based, was similar, they differed when sCT was included. In fact, the surfaces of the particles made of B-PEG were more folded and rougher than those of the particles made of L-PEG.

Solid state analysis.

X-ray diffractograms and DSC thermograms of sCT loaded particle are shown in Figure 7E and Figure 7F, respectively. They did not show the presence of Bragg peaks and melting endotherm specific to sCT. Whereas PVP seemed to have a low impact on the PEG relative degree of crystallinity, the addition of 4.8 wt% of sCT decreased it, as suggested by the diminution of the area of the diffraction Bragg peaks and melting peaks on the diffractograms and thermograms, respectively. The relative degree of crystallinity of PEG in sCT loaded particles, calculated using Equation (1) was $75.2 \pm 3.8\%$ and $75.6 \pm 4.1\%$ for B-PEG and L-PEG based particles, respectively. These relative degrees of crystallinity values were significantly lower than those calculated for the blank B-PEG and L-PEG based particles, $91.8 \pm 4.6\%$ and $90.5 \pm 4.7\%$ respectively, when compared using the t-test ($p > 0.05$). Diminution of PEG relative degree of crystallinity in the presence of sCT was not different between particles made of L-PEG or B-PEG. However, whereas the L-PEG melting peak temperature was not affected by the presence of sCT, it was shifted to a lower temperature for the B-PEG (Fig. 7F).

Dynamic vapour sorption.

Water vapour sorption isotherms of sCT loaded particles formulated with L-PEG and B-PEG are shown in Figure 9A and 9B, respectively. These particles uptake the same relative amount of water as the blank particles, and similarly the isotherms showed an adsorption mechanism dominated by type II behaviour of the IUPAC classification. Both types of particle captured similar relative amount of water, but the isotherm obtained with B-PEG-based particles presented a closed hysteresis loop in its upper part, whereas the adsorption and desorption branches of the isotherm obtained with L-PEG based particle were similar. Furthermore, for the two formulations, the water uptake kinetic profiles obtained for 60 and 70 %RH showed a decrease in mass versus time instead of an increase followed by a plateau (see inserts in Fig. 9). This event is usually due to the crystallisation of an amorphous compound (Buckton and Darcy, 1995), as crystalline phases are less hydrophilic than amorphous ones.

Particle size distribution and aerodynamic properties.

The average D_{50} of the sCT loaded particle size distribution in volume and their aerodynamic properties are illustrated in Figure 10. No significant differences in particle size distributions and aerodynamic properties were observed for particles formulated using either B-PEG or L-PEG. Compared to blank particles, D_{50} and MMAD of the B-PEG-based sCT loaded particles were not significantly different, whereas they were significantly increased for the L-PEG-based particles ($p < 0.05$, t-test). Interestingly, the average FPF of B-PEG-based sCT loaded particles was significantly higher than the equivalent blank particles ($p < 0.05$, t-test). No significant differences were observed in the FPF calculated for the B-PEG and L-PEG-based sCT loaded particles.

sCT loading.

Loading and loading efficiency values of the sCT loaded particles formulated with linear and B-PEG are shown in Table 2. Targeting a loading of 4.8 wt% resulted in a high loading efficiency for the two formulations: $77.9 \pm 2.3\%$ and $83.6 \pm 1.4\%$ for the L-PEG and B-PEG-based particles, respectively. However, the loading efficiency obtained with the B-PEG-based particles was significantly higher than that obtained with the L-PEG-based particles ($p < 0.05$, *t*-test).

Bioactivity.

The bioactivity of sCT after co-processing with L-PEG and B-PEG-based was measured indirectly by assessing cAMP release from T47D cells (Fig. 11). It could be observed that the bioactivity of sCT was not significantly affected in the 10^{-5} – 10^{-7} M concentration range, showing that the process as well as the excipients did not impact on the integrity of the peptide. Furthermore, these formulations demonstrated the ability to maintain the peptide activity over a period of at least 2 months when stored at 4°C.

3. Discussion.

3.1. Blank particles.

PEG polymers solidify in a crystalline or semi-crystalline state having a low melting and glass transition temperature (Verheyen *et al.*, 2001). Hence, they are difficult to process alone by spray drying as they form sticky fused materials in the warm spray dryer (Corrigan *et al.*, 2002). The morphology of the L-PEG/PVP particles observed by SEM showed a decrease in particle fusion with an increase in PVP content. The decrease in particle fusion can be attributed to the protecting effect of PVP during the spray drying process. This polymer having a T_g (110°C) higher than the T_m of the PEG polymers and higher than the outlet temperature in the spray dryer prevents the particles from fusing. Two phenomena can explain this result. The first possibility is the development of interactions between PVP and PEG, increasing the T_g of the blend of polymer. The second possibility is that the PVP is present in a sufficient amount at the surface of the particles to inhibit their fusion. The small decrease in PEG relative degree of crystallinity in the particles favours the latter theory and indicates an increase in the PVP surface concentration when the whole PVP amount was increased in the polymer system. The PVP/PEG ratio also influenced the particles' surface. For 50 wt% of PVP, particle surfaces were rough and presented some convolutions (Fig. 1C'). This kind of surface is favourable for particle aerosolisation as it should help to reduce particle interactions and increase dragging forces responsible for sustaining the particles in the air stream of the patients during inspiration. An increase in the proportion of acetone up to 85 wt% in the spray dried solutions led to the formation of hollow particles with a rough surface. The formation of hollow particles should decrease the particle apparent density and help to reduce the MMAD. Changing the L-PEG to B-PEG of the same M_w modified the particles behaviour in the spray dryer. Mixing with 50% PVP and in the presence of 50 wt% of

acetone in the spray dried solution, a condition which resulted in isolated rough surface particles with the L-PEG, resulted in fused particles using B-PEG. For the B-PEG, 70% of acetone in the spray dried solution was required to formulate isolated particles, having a rough surface. As B-PEG has a different conformation to L-PEG, they could have different molecular diameters and diffusion coefficients in solution. Thus B-PEG may require more acetone in the spray dried solution in order to get faster PVP precipitation and accumulation at the surface.

Particle – water interactions.

Because the amount of free water in a powder influences its physical stability and controls the magnitude of capillary forces that hold particles in aggregates, thereby controlling the respirability of the powder, TGA and DVS analysis were performed in order to evaluate how and to what extent water molecules interact with the particles. The mass loss from the L-PEG-based particles observed by TGA at relatively low temperature (between 20°C and 60°C) could be attributed to desorption of solvent from the polymer particle surface (Ghosh *et al.*, 1999, Haddadine-Rahmoun *et al.*, 2008). As the mass loss increased as the PVP amount increased in the particles, PVP molecules present at the surface of the particles could be responsible for the increase in solvent uptake.

Water sorption isotherms obtained with the spray dried L-PEG/PVP systems showed a transition from the type III to the type II behaviour of the IUPAC classification (IUPAC, 1986) with an increase in the PVP amount. Usually, the differences between type II and III behaviours are due to differences in the sorption enthalpy of the solvent. If the vapour molecule has a strong interaction with the solid surface in comparison to the interaction with other vapour molecules, the vapour adsorbs on the surface as a monolayer; if the surface is homogeneous. After completion of the monolayer, condensation of vapour molecules in multilayers can occur,

resulting in a type II isotherm. When the vapour molecules interact with the surface with a similar energy to the interaction developed with another vapour molecule, only very few molecules adsorb at the solid surface at low partial pressures. Then at higher partial pressures, vapour molecules condense on the few initially adsorbed molecules, leading to type III behaviour. For the isotherms obtained with L-PEG – PVP systems, the higher the PVP content, the more the shape of the isotherms at low %RH, related to surface water adsorption, was similar to that obtained with the PVP raw material. This suggests that an increase in PVP concentration in the PEG-PVP system resulted in an increase in the PVP concentration at the particle surface.

Additionally, isotherms obtained with L-PEG/PVP particles exhibit closed hysteresis loops, that is, the amount of water associated with the particles was greater for the desorption isotherm than for the sorption isotherm at a given %RH. Hysteresis of sorption isotherms can have various causes. Some of the fundamental mechanisms include capillary condensation in porous material, hydrate formation or bulk sorption (Alvarez-Lorenzo *et al.*, 2000). In some cases a combination of these effects can occur. At high %RH, hysteresis loops are often due to the porous structure of the material (Kachrimanis *et al.*, 2006). The appearance of a hysteresis loop at high %RH with the increase in the PVP amount to 50 wt% could be explained by the increase in the particles' surface porosity in this formulation, whereas other formulations displayed a smooth surface. This was in accordance with the SEM micrographs (Fig. 1).

However, amorphous or partially amorphous polymers, such as PVP and PEG, are structurally rather complex, and interpretation of hysteresis effects is not trivial. A number of explanations have been proposed based on experiments performed on cellulose and starch derivatives (Zografis and Kontny, 1986). For instance, hysteresis may be due to changes in polymer chain conformation (irreversible swelling) or to an increase in the strength of solid–liquid bonding.

These phenomena would be mediated by the entry of water into the polymeric structure. The built-up surface condensed water can act as a driving force to cause water to penetrate into the bulk of the polymer particle during sorption but not during desorption resulting in the different moisture contents following sorption or desorption at the same %RH (Agrawal *et al.*, 2004). In fact, amorphous or semi-crystalline materials tend to exhibit considerable bulk absorption of water which may result in swelling effects (Agrawal *et al.*, 2004, Alvarez-Lorenzo *et al.*, 2000, Bravo-Osuna *et al.*, 2005). Hence, the distribution of moisture in various forms (adsorbed or absorbed) has been determined by using the Young and Nelson equations. Results indicate that for the L-PEG, absorption at high %RH represents the main way in which water was taken up. This bulk water could have an effect on particle chemical stability and swelling. In contrast, for the PVP raw material, adsorption of water as a monolayer at low %RH and then as multilayers at high %RH was the main way in which water interacts with the polymer. PVP also absorbed water molecules in a linear manner in the range of %RH investigated. In the L-PEG – PVP systems, as the proportion of PVP increased, the percentage of adsorbed water increased, which might be expected to result in the aggregation of particles. Hence, a high content of PVP at the surface of the particles should disimprove aerosolisation properties. Furthermore, the PVP present in the particles increases their capacity of absorbing water at low %RH. This could result in particles swelling and to an increase in their geometric diameter, adversely impacting their aerodynamic properties. In contrast, an increase in PEG proportion in the polymer system increased the minimal %RH required to trigger the water absorption process, protecting particles from swelling at usual ambient RH. These experiments highlight that, in order to use PVP and PEG to protect proteins and peptides from denaturation and in the same time maintain a low cohesiveness between the particles, an appropriate PEG/PVP ratio has to be found.

Solid state analysis

The solid state of a powder can affect the aerosolisation properties as a component in the crystalline state should be less cohesive than in the amorphous state (Chow *et al.*, 2007). In fact, the dispersive surface energy of a material is higher in the amorphous state than in the crystalline state. However, material density is usually lower in the amorphous compared to the crystalline state. Thus individual particles made of amorphous materials may have a larger aerodynamic diameter than the crystalline equivalent particles. Additionally, a crystalline state of excipients can be detrimental for protein stability because of phase separation and loss of excipient–protein interaction (Bosquillon *et al.*, 2004). Therefore, we analyzed the relative degree of crystallinity of the PEG in the particles by X-ray diffraction and DSC. According to these experiments, the variation of the L-PEG/PVP ratio in the particle has a low effect on the relative degree of crystallinity of L-PEG in the polymer systems. Additionally, the small decrease in the relative degree of crystallinity could be attributed in part to the spray drying process. Corrigan *et al.* (2002) observed that a reduction in crystallinity of ~ 10–15 wt% of PEG 4000 was achieved on spray drying. Therefore, an increase in the PVP/PEG ratio has a minor effect on the L-PEG relative degree of crystallinity. This illustrated the absence, or the negligible degree of interaction, between the PEG and PVP polymer. Similarly, the relative degree of crystallinity of linear PEG 6kDa remained higher than 80% when co-spray dried with 75 wt% of PVP K25 (Janssens *et al.*, 2008). Also, Cesteros *et al.* (1989) showed that high molecular weight PVP and PEG of 24 kDa and 32 kDa, respectively, were immiscible.

An increase in the concentration of acetone in the spray dried solution did not influence the relative degree of crystallinity of the L-PEG in the PEG-PVP systems, as observed by XRD and DSC. The high values of relative degree of crystallinity of the L-PEG in the polymer blend,

calculated for particles formulated from solutions composed of 70 and 85 wt% of acetone is consistent with a low degree of interaction between the PVP and the L-PEG in the particles.

As was the case for the L-PEG raw material, the B-PEG raw material was also crystalline. The melting endotherm for B-PEG was characterised by a concave melting curve, starting at 44°C that was much lower than the peak temperature (61.7°C), suggesting the existence of various B-PEG chain organisations in the crystal, as previously observed for linear PEG 6kDa (Verheyen *et al.*, 2001, Verheyen *et al.*, 2002). The relative degree of crystallinity of B-PEG in the polymer systems calculated using the melting enthalpies were still high and, when subjected to the same processing conditions, not significantly different of the relative degree of crystallinity of L-PEG. The changes in water/acetone ratio in the spray dried solution did not affect the peak position. However, the presence of PVP shifted the melting endotherm of the B-PEG by ~ 8°C to a lower temperature. This could be attributed to a change in the B-PEG chains conformation, as was observed for the PEG 6kDa (Verheyen *et al.*, 2001), due to the presence of some interaction with the PVP or due to the spray drying process.

Particle size distribution and aerodynamic properties

In the case of L-PEG/PVP, particles composed of 50 and 70 wt% of PVP and spray dried from a solution composed of 50 wt% of acetone displayed similar D_{50} , and appeared to be suitable for inhalation as they were less than 5 μm . Their approximate theoretical MMAD can be calculated based on the D_{50} of the geometric particle size distribution, the particle shape and the particle density using the following relation:

$$\text{MMAD} = D_{50} \sqrt{\frac{\rho}{\chi \rho_0}}, \text{ where } \rho_0 \text{ is the unit density (1 g. cm}^{-3}\text{), } \rho \text{ is the particle density and } \chi \text{ is}$$

the dynamic shape factor. The dynamic shape factor is defined as the ratio of the drag force on a particle to the drag force on the volume-equivalent sphere having a smooth surface at the same

velocity. Hence, the spherical PEG/PVP particles having a rough surface should have $\chi \geq 1$. The density of crystalline PEG is 1.227 g. cm^{-3} while the density of amorphous PEG is dependent upon the temperature (Brandrup *et al.*, 1999). The density of amorphous PEG at $30 \text{ }^\circ\text{C}$ was estimated to be 1.118 g. cm^{-3} (Brandrup *et al.*, 1999). PVP density at 25°C was measured as 1.228 g. cm^{-3} using helium pycnometer. Thus particle density should be $\sim 1.22 \text{ g. cm}^{-3}$, and theoretical MMAD $\sim 3.7 \text{ }\mu\text{m}$ (for $\chi = 1$). A comparison of the MMAD obtained by the NGI and this calculated MMAD indicated that powder aerosols exited the Handihaler[®] inhaler as particle aggregates rather than isolated particles. The degree of particles aggregation was lower with the particles composed of 50 wt% of PVP than those composed 70 wt%, as their MMAD were significantly different (7.3 and $11.6 \text{ }\mu\text{m}$, respectively). This difference in MMAD could be attributed to the lower water adsorption at the ambient %RH of particles made of 50 wt% of PVP in comparison to those made of 70 wt% of PVP. Additionally, the higher surface roughness of the particles made of 50% of PVP should enhance their aerodynamic properties. On the other hand, these two kinds of particles displayed the same FPF. The absence of significant differences between the FPF values obtained for the particles made of 50 wt% and 70 wt% of PVP can be attributed to the large aerodynamic particle diameter distribution of the formulation made with 70 wt% of PVP, characterised by a large average GSD of 3.1 ± 0.7 in comparison to the aerodynamic diameter distribution obtained for the particles made of 50 wt% of PVP. Additionally, this absence of difference could also be attributed to the large distribution of the FPF values calculated for the formulation based on 70 wt% of PVP, characterised by a high SD (CV=40%). Although particles exited the inhaler as aggregates, their porosity and perhaps their low densities resulted in a large fraction of particle aggregates with an aerodynamic size lower than $5 \text{ }\mu\text{m}$ as their FPF were $> 20\%$. Nevertheless, particles formulated with 50% of L-PEG are

expected to penetrate deeper in the lung and produce more reproducible aerosol deposition than those made of 70 wt% of PVP. An increase in wt% of acetone in the spray dried solution did not affect D_{50} , but it resulted in a narrowing of the geometric particle size distribution. Additionally, the increase in acetone concentration up to 70% led to a significant decrease in the average MMAD and increase in the average FPF to 32% in comparison to the values obtained with 50 wt% of acetone. Therefore, an increase in the acetone concentration from 50 to 70 wt% allowed particles with better aerodynamic properties to be formulated; particles should penetrate deeper in the lung and in higher proportion.

In the case of particles comprising B-PEG, an increase in acetone concentration to 70 wt% of spray dried solution allowed the production of particles having a monomodal size distribution but with an average D_{50} significantly larger than particles made of L-PEG. MMAD and FPF of the L-PEG based particle were significantly lower and higher, respectively, than the B-PEG based particles, Hence, the use of L-PEG allowed to formulate sCT-free particles with better aerodynamic characteristics than those obtained with the B-PEG of equivalent molecular weight.

3.2. Salmon calcitonin loaded particles.

The development of particles for the systemic administration of high potent protein or peptides via pulmonary route often require the use of bulking/stabilising excipients, e.g. hygroscopic sugars such as mannitol or trehalose, which can interact and protect the peptide to produce a stable powder. In order to evaluate the capacity of the B-PEG and L-PEG based particles to deliver and stabilise sCT, two types of sCT-loaded particles were formulated with these polymers. The morphology of the sCT loaded particles was changed in contrast to the sCT-free particles; in particular, the surface of the sCT-loaded particles looked less nanoporous and more folded. Whereas the morphology of blank particles made of B-PEG and L-PEG were similar,

they were different in the presence of sCT. The surfaces of the particles made of B-PEG were more folded and rougher than those made of L-PEG. This folded structure of the sCT-loaded particles should improve their aerodynamic behaviour.

Solid state analysis

No evidence of crystallisation of sCT in the particles was observed, indicating that the peptide remained amorphous during the spray drying process. Likewise sCT was amorphised when co-spray dried with mannitol (Chan *et al.*, 2004). Whereas PVP seemed to have a low impact on the relative degree of crystallinity of the two PEGs, the addition of 4.8 wt% of sCT significantly decreased their relative degree of crystallinity. The level of crystallinity reduction did not differ between particles made of L-PEG or B-PEG. However, whereas the L-PEG melting peak temperature was not affected by the presence of sCT, it was shifted to a lower temperature for the B-PEG (Fig. 7F). The decrease of PEG relative degree of crystallinity in the presence of sCT suggests the development of interactions between these molecules which may help to protect sCT against unfolding and denaturation.

Particle – water interactions.

Whereas, particles made of B-PEG and L-PEG captured similar relative amounts of water, B-PEG-based particles presented a higher water sorption hysteresis than particles made of L-PEG. This distinction could be attributed to the difference in the particle surface roughness/porosity (IUPAC, 1986). In fact, the surface of the sCT loaded particles made with B-PEG was more folded than those of the particles made with L-PEG. Another phenomenon observed on the isotherms was the water uptake kinetic profiles obtained for 60 and 70 %RH showing a decrease in mass versus time (Fig. 9). This event is usually due to the crystallisation of an amorphous compound (Buckton and Darcy, 1995), as crystalline phases are less hydrophilic than amorphous

ones. In these experiments the crystallisation can be attributed to the proportion of amorphous PEG (linear or branched) present in the sCT loaded particles. XRD and DSC experiments performed on sCT loaded particles after the DVS experiments, demonstrated that the PEG relative degree of crystallinity in these particles increased back to the same values as those found for the blank particles. This PEG crystallisation could be responsible for the overlapping of the sorption and desorption isotherm branches, creating two closed loops in the lower part of the isotherms. A similar phenomenon was also observed with mannitol-sCT particles formulated by spray drying, as mannitol crystallised when particles were exposed to 60% of RH (Chan *et al.*, 2004). This recrystallisation of the PEG induced by the moisture could impair the sCT stability, and suggest that particles should be kept at a %RH lower than 60%.

Particle size distribution and aerodynamic properties

Compared to blank particles, D_{50} and MMAD of B-PEG-based sCT loaded particles were not significantly different, whereas D_{50} and MMAD of sCT loaded particles formulated with L-PEG were significantly higher than the equivalent sCT-free particles. Hence, this increase in MMAD could be mainly attributed to an increase in particle size rather than to an increase in particle cohesiveness. The slightly high MMAD values, at around 7 μm , could result in a low lung administration efficiency. However, due to their high GSD values, MMAD values are of less significance in predicting alveolar and lung deposition since, as was observed by Finlay *et al.* (Finlay *et al.*, 1997), with high GSD values, the inhaled fine particle mass is almost constant over a wide range of MMADs between 1.0 and 9.0 μm . Furthermore, the FPF of the two PEG-based sCT loaded formulation was higher than 32%. These FPF values were considered acceptable for peptide loaded particles. In fact, a previously commercialised product made of insulin (ExuberaTM) had a FPF around 22% (de Boer *et al.*, 2008), although it should be highlighted that

FPF values are dependent on the type of inhaler and on the flow rate used (Frijlink and De Boer, 2004).

Particles loading

Loading efficiencies were high for the formulations made of L-PEG and B-PEG, at around 80%. However, the loading efficiency obtained with the B-PEG-based particles was significantly higher than that obtained with the L-PEG-based particles. This, added to the high spray drying yield obtained using B-PEG, makes it a better excipient to formulate peptide-loaded microparticles.

Bioactivity

sCT bioactivity was maintained for more than 2 months when particles were stored at 4°C in a refrigerator. The maintenance of the whole activity of the peptide was one of the main goals of the study. This is an important finding since other studies reported a significant chemical degradation and sCT aggregation when a spray-dried powder of pure sCT was stored at 25°C and 75% RH for 7 days (Lechuga-Ballesteros *et al.*, 2008).

4. Conclusions

This study offered a new approach to the formulation of active peptide loaded microparticles suitable for pulmonary administration. This study showed that L-PEG or B-PEG can not be spray dried alone to produce particles suitable for aerosolisation due to their low T_m . When PVP K15 and L-PEG or B-PEG of 10kDa were co-spray dried the polymers solidified in separate phases. Also, increasing weight ratio of PVP in the system resulted in the amount of PVP on the particle surfaces to be increased, protecting them against fusion during the spray drying process, due to the relatively high T_g of the PVP. However, PVP was found to be more hygroscopic than the PEG polymers in an atmospheric %RH range. Reduced aerodynamic properties of particles containing higher PVP content may be attributed to an increase in capillary forces between the particles. Hence, an optimal proportion between PEG and PVP of 50 wt% each was found to optimise particle aerodynamic properties.

The use of acetone in the spray dried solution allowed the outlet temperature in the spray dryer to be decreased and additionally facilitated the PVP solidification as it is a poor solvent for this polymer. Hence increasing the amount of poor solvent for the PVP up to 70 wt% in the spray dried solution allowed the solidification to be accelerated and resulted in the formulation of particles with a narrower monodisperse size distribution. This study demonstrated that particle surface properties can be adjusted by altering the water/acetone and PEG/PVP ratio in the spray dried solution.

Targeting a 5 wt% of sCT loading resulted in a loading efficiency of 77.9 and 83.6 % with L-PEG and B-PEG based particles, respectively. The higher sCT loading efficiency and the higher spray drying yield obtained with the B-PEG in comparison to the linear one could be attributed to a higher degree of interaction between the B-PEG and the sCT. In fact, whereas the PVP had

very little effect on PEG relative degree of crystallinity, the inclusion of only 5 wt% of sCT significantly decreased it, in addition to modifying the particle surface morphology and aerodynamic properties. This decrease in PEG crystallinity impairs the formulation stability as the small amount of amorphous PEG created recrystallises when the %RH reaches 60%. The use of B-PEG resulted in a rougher surface for the sCT-loaded particles than with L-PEG. However, this morphological change did not significantly influence the aerodynamic particle properties, which were considered as suitable for aerosolisation of peptide since FPFs were higher than 30 %. Interestingly, these particles were able to maintain sCT activity for more than 2 months, as evaluated by the production of cAMP by the T47D cells. This is an important finding and provides a justification for the use of excipients when spray drying sCT.

Acknowledgements

The authors want to thank Prof. David J. Brayden and Dr. Sinead Ryan (University College Dublin, Ireland) for the T47D cells and their advice regarding the sCT bioactivity assay. This study was funded by the Irish Drug Delivery Research Network, a Strategic Research Cluster grant (07/SRC/B1154) under the National Development Plan co-funded by EU Structural Funds and Science Foundation Ireland.

References

- Agrawal, A., M. , Manek, R., V. , Kolling, W., M., Neau, S., H., 2004. Water distribution studies within microcrystalline cellulose and chitosan using differential scanning calorimetry and dynamic vapor sorption analysis. *Journal of Pharmaceutical Sciences*. 93, 1766-1779.
- Alvarez-Lorenzo, C., Gómez-Amoza, J. L., Martínez-Pacheco, R., Souto, C., Concheiro, A., 2000. Interactions between hydroxypropylcelluloses and vapour/liquid water. *European Journal of Pharmaceutics and Biopharmaceutics*. 50, 307-318.
- Bailon, P., Berthold, W., 1998. Polyethylene glycol-conjugated pharmaceutical proteins. *Pharmaceutical Science and Technology Today*. 1, 352-356.
- Bosquillon, C., Rouxhet, P. G., Ahimou, F., Simon, D., Culot, C., Pr at, V., Vanbever, R., 2004. Aerosolization properties, surface composition and physical state of spray-dried protein powders. *Journal of Controlled Release*. 99, 357-367.
- Brandrup, J., Immergut, E. H., Grulke, E. A., 1999. *Polymer Handbook*.
- Bravo-Osuna, I., Ferrero, C., Jim nez-Castellanos, M. R., 2005. Water sorption-desorption behaviour of methyl methacrylate-starch copolymers: effect of hydrophobic graft and drying method. *European Journal of Pharmaceutics and Biopharmaceutics*. 59, 537-548.
- Buckton, G., Darcy, P., 1995. The use of gravimetric studies to assess the degree of crystallinity of predominantly crystalline powders. *International Journal of Pharmaceutics*. 123, 265-271.
- Cesteros, L. C., Quintana, J. R., Fernandez, J. A., Katime, I. A., 1989. Miscibility of poly(ethylene oxide) with poly(N-vinyl pyrrolidone). DMTA and DTA studies. *Journal of Polymer Science, Part B: Polymer Physics*. 27, 2567-2576.
- Chan, H. K., Clark, A. R., Feeley, J. C., Kuo, M. C., Lehrman, S. R., Pikal-Cleland, K., Miller, D. P., Vehring, R., Lechuga-Ballesteros, D., 2004. Physical Stability of Salmon Calcitonin Spray-Dried Powders for Inhalation. *Journal of Pharmaceutical Sciences*. 93, 792-804.
- Cheng, W., Lim, L.-Y., 2009. Lipeo-sCT: A novel reversible lipidized salmon calcitonin derivative, its biophysical properties and hypocalcemic activity. *European Journal of Pharmaceutical Sciences*. 37, 151-159.
- Chow, A. H. L., Tong, H. H. Y., Chattopadhyay, P., Shekunov, B. Y., 2007. Particle engineering for pulmonary drug delivery. *Pharmaceutical Research*. 24, 411-437.

- Corrigan, D. O., Corrigan, O. I., Healy, A. M., 2004. Predicting the physical state of spray dried composites: Salbutamol sulphate/lactose and salbutamol sulphate/polyethylene glycol co-spray dried systems. *International Journal of Pharmaceutics*. 273, 171-182.
- Corrigan, D. O., Healy, A. M., Corrigan, O. I., 2002. The effect of spray drying solutions of polyethylene glycol (PEG) and lactose/PEG on their physicochemical properties. *International Journal of Pharmaceutics*. 235, 193-205.
- D'souza, A. J. M., Schowen, R. L., Topp, E. M., 2004. Polyvinylpyrrolidone-drug conjugate: Synthesis and release mechanism. *Journal of Controlled Release*. 94, 91-100.
- De Boer, A., Hagedoorn, P., Schellekens, R., Rottier, B., Bocca, G., Duiverman, E., Frijlink, H., 2008. Can Systemic Drug Delivery via the Pulmonary Route be Achieved Effectively with a Dry Powder Inhaler? *Lessons Learned from Exubera. Drug Delivery to the Lungs* 19. 27-30.
- Edwards, D. A., Dunbar, C., 2002. Bioengineering of therapeutic aerosols. *Annual Review of Biomedical Engineering*. 4, 93-107.
- Fee, C. J., 2007. Size comparison between proteins PEGylated with branched and linear poly(ethylene glycol) molecules. *Biotechnology and Bioengineering*. 98, 725-731.
- Filpula, D., Zhao, H., 2008. Releasable PEGylation of proteins with customized linkers. *Advanced Drug Delivery Reviews*. 60, 29-49.
- Finlay, W. H., Stapleton, K. W., Zuberbuhler, P., 1997. Fine particle fraction as a measure of mass depositing in the lung during inhalation of nearly isotonic nebulized aerosols. *Journal of Aerosol Science*. 28, 1301-1309.
- Frijlink, H. W., De Boer, A. H., 2004. Dry powder inhalers for pulmonary drug delivery. *Expert Opinion on Drug Delivery*. 1, 67-86.
- Ghosh, P., Siddhanta, S. K., Chakrabarti, A., 1999. Characterization of poly(vinyl pyrrolidone) modified polyaniline prepared in stable aqueous medium. *European Polymer Journal*. 35, 699-710.
- Haaf, F., Sanner, A., Straub, F., 1984. Polymers of N-vinylpyrrolidone: synthesis, characterization and uses. *Polymer Journal*. 17, 143-152.
- Haddadine-Rahmoun, N., Amrani, F., Arrighi, V., Cowie, J. M. G., 2008. Interpolymer complexation and thermal behaviour of poly(styrene-co-maleic acid)/poly(vinyl pyrrolidone) mixtures. *Thermochimica Acta*. 475, 25-32.
- Healy, A. M., McDonald, B. F., Tajber, L., Corrigan, O. I., 2008. Characterisation of excipient-free nanoporous microparticles (NPMPs) of bendroflumethiazide. *European Journal of Pharmaceutics and Biopharmaceutics*. 69, 1182-1186.

- Iupac, 1986. Reporting physisorption data for Gas/solid systems with special reference to the determination of surface area and porosity. *Pure and Applied Chemistry*. 57, 603-619.
- Janssens, S., Novoa De Armas, H., Roberts, C. J., Van Den Mooter, G., 2008. Characterization of ternary solid dispersions of itraconazole, PEG 6000, and HPMC 2910 E5. *Journal of Pharmaceutical Sciences*. 97, 2110-2120.
- Jirgensons, B., 1952. Solubility and fractionation of polyvinylpyrrolidone. *Journal of Polymer Science*. 8, 519-527.
- Kachrimanis, K., Noisternig, M. F., Griesser, U. J., Malamataris, S., 2006. Dynamic moisture sorption and desorption of standard and silicified microcrystalline cellulose. *European Journal of Pharmaceutics and Biopharmaceutics*. 64, 307-315.
- Kompella, U. B., Lee, V. H. L., 2001. Delivery systems for penetration enhancement of peptide and protein drugs: Design considerations. *Advanced Drug Delivery Reviews*. 46, 211-245.
- Lechuga-Ballesteros, D., Charan, C., Stults, C. L. M., Stevenson, C. L., Miller, D. P., Vehring, R., Tep, V., Kuo, M. C., 2008. Trileucine improves aerosol performance and stability of spray-dried powders for inhalation. *Journal of Pharmaceutical Sciences*. 97, 287-302.
- Lucas, P., Anderson, K., Staniforth, J. N., 1998. Protein deposition from dry powder inhalers: Fine particle multiplets as performance modifiers. *Pharmaceutical Research*. 15, 562-569.
- Mitri, J., Pittas, A. G., 2009. Inhaled insulin - What went wrong. *Nature Clinical Practice Endocrinology and Metabolism*. 5, 24-25.
- Nolan, L. M., Tajber, L., McDonald, B. F., Barham, A. S., Corrigan, O. I., Healy, A. M., 2009. Excipient-free nanoporous microparticles of budesonide for pulmonary delivery. *European Journal of Pharmaceutical Sciences*. 37, 593-602.
- Patton, J., 1998. Breathing life into protein drugs. *Nature Biotechnology*. 16, 141-143.
- Pean, J. M., Boury, F., Venier-Julienne, M. C., Menei, P., Proust, J. E., Benoit, J. P., 1999. Why does PEG 400 co-encapsulation improve NGF stability and release from PLGA biodegradable microspheres? *Pharmaceutical Research*. 16, 1294-1299.
- Pharmacopoeia, 2009. Appendix XII C: Aerodynamic Assessment of Fine Particles - Fine Particle Dose and Particle Size Distribution. *British Pharmacopoeia*. IV,
- Reddy, R., Chang, L., Luthra, S., Collins, G., Lopez, C., Shamblin, S. L., Pikal, M. J., Gatlin, L. A., Shalaev, E. Y., 2009. The glass transition and sub-Tg-relaxation in

- pharmaceutical powders and dried proteins by thermally stimulated current. *Journal of Pharmaceutical Sciences*. 98, 81-93.
- Ryan, S. M., Wang, X., Mantovani, G., Sayers, C. T., Haddleton, D. M., Brayden, D. J., 2009. Conjugation of salmon calcitonin to a combed-shaped end functionalized poly(poly(ethylene glycol) methyl ether methacrylate) yields a bioactive stable conjugate. *Journal of Controlled Release*.
- Seville, P. C., Li, H. Y., Learoyd, T. P., 2007. Spray-dried powders for pulmonary drug delivery. *Critical Reviews in Therapeutic Drug Carrier Systems*. 24, 307-360.
- Verheyen, S., Augustijns, P., Kinget, R., Van Den Mooter, G., 2001. Melting behavior of pure polyethylene glycol 6000 and polyethylene glycol 6000 in solid dispersions containing diazepam or temazepam: A DSC study. *Thermochimica Acta*. 380, 153-164.
- Verheyen, S., Blaton, N., Kinget, R., Van Den Mooter, G., 2002. Mechanism of increased dissolution of diazepam and temazepam from polyethylene glycol 6000 solid dispersions. *International Journal of Pharmaceutics*. 249, 45-58.
- Vicent, M. J., Duncan, R., 2006. Polymer conjugates: Nanosized medicines for treating cancer. *Trends in Biotechnology*. 24, 39-47.
- Yoshioka, S., Aso, Y., Miyazaki, T., 2006. Negligible contribution of molecular mobility to the degradation rate of insulin lyophilized with poly(vinylpyrrolidone). *Journal of Pharmaceutical Sciences*. 95, 939-943.
- Youn, Y. S., Jung, J. Y., Oh, S. H., Yoo, S. D., Lee, K. C., 2006. Improved intestinal delivery of salmon calcitonin by Lys18-amine specific PEGylation: Stability, permeability, pharmacokinetic behavior and in vivo hypocalcemic efficacy. *Journal of Controlled Release*. 114, 334-342.
- Youn, Y. S., Kwon, M. J., Na, D. H., Chae, S. Y., Lee, S., Lee, K. C., 2008. Improved intrapulmonary delivery of site-specific PEGylated salmon calcitonin: optimization by PEG size selection. *Journal of Controlled Release*. 125, 68-75.
- Zografi, G., Kontny, M. J., 1986. The interactions of water with cellulose- and starch-derived pharmaceutical excipients. *Pharmaceutical Research*. 3, 187-194.

Table 1: Estimated *A* and *B* Young and Nelson parameters.

	<i>A x 100</i>	<i>B x 100</i>
Linear PEG	1.2	40.2
15% PVP	2.0	50.1
30% PVP	4.3	54.9
50% PVP	7.0	60.2
70% PVP	9.9	11.1
PVP	13.0	8.0

Table 2: sCT loading in the polymeric particles

	Loading %	Loading efficiency %	Spray drying yield %
L-PEG	3.73±0.11	77.9±2.3	69
B-PEG	3.94±0.07	83.6±1.4	80

Figure 1: SEM micrographs of particles formulated by spray drying solutions having a 1/1 (w/w) acetone/water ratio. PVP/L-PEG weight ratio was varied from (A) 0.15, (B) 0.30, (C) 0.50 and (D) 0.70. (C') and (D') are higher magnifications of (C) and (D).

Figure 2: Water vapour sorption-desorption isotherms obtained with formulations made of various weight ratios of L-PEG-PVP or with the polymer raw material. Temperature was 25°C. Isotherms are expressed as percentage of the weight uptake with the dry mass taken as reference. Insert shows a magnified view of isotherms at low % of RH.

Figure 3: Example of Young and Nelson isotherm fitting results obtained with the PVP raw material.

Figure 4: (A) X-ray diffraction pattern of particles made with various ratios of L-PEG – PVP. Particles were formulated by spray drying solutions containing 1 wt% of polymer and having a 1/1 (w/w) acetone/water ratio. (B) DSC thermograms. (C) Relative degree of crystallinity of L-PEG in the “PVP-L-PEG” polymer systems after spray drying. Values were calculated using Eq. 1 and the melting enthalpy of the PEG raw material, $\Delta H_{fPEG} = 183.5 \text{ J/g}$.

Figure 5: Micromeritic and aerodynamic properties of PVP/L-PEG particles having different PEG/PVP ratios. A) Volume median diameter of the particle size distribution determined by laser diffraction B) Mass median aerodynamic diameter C) Geometric standard deviation of the aerodynamic particle size distributions D) Fine particle fraction expressed as percentage of the recovered particles. Particles were formulated by spray drying solutions containing 1 wt% of L-

PEG - PVP polymers and composed of acetone and water in a 1/1 (w/w) ratio. Data are the average of 3 measurements. ** (P < 0.01), * (P < 0.05). (ND: Not determined).

Figure 6: SEM micrographs of particles made in PEG/PVP weight ratio of 1. (A), (B) and (E) were made of L-PEG; (C), (D) and (F) were made of B-PEG. Spray dried solution contained: (A) 70 wt% of acetone, (B) 85 wt% of acetone (C) 50 wt% of acetone and (D) 70 wt% of acetone. (E) and (F) were loaded with 5 wt% of sCT. Loaded particles were formulated from solutions composed of 70 wt% of acetone as (A) and (D).

Figure 7: XRD patterns (A, C, D) and DSC thermograms (B, D, F) of formulations made of 1/1 (w/w) PEG/PVP and various acetone concentration of the spray dried solutions. (A), (B) were made of L-PEG; (C), (D) were made of B-PEG. (E) and (F) compared results obtained with blank and loaded (5 wt%) formulations. Loaded particles were formulated from solutions composed of 70 wt% of acetone.

Figure 8: Micromeritic and aerodynamic properties of particles made of PVP and L-PEG or B-PEG. Particles were formulated by spray drying solutions containing 1 wt% of PEG – PVP polymers and composed of different acetone/water weight ratios. A) Volume median diameter of the particle size distribution determined by laser diffraction B) Mass median aerodynamic diameter C) Geometric standard deviation of the aerodynamic particle size distribution D) Fine particle fraction expressed as percentage of the recovered particles. Data are the average of 3 measurements. ** (P < 0.01), * (P < 0.05). (ND: Not determined).

Figure 9: Vapour sorption-desorption isotherms obtained with sCT-loaded particles A) L-PEG based particles B) B-PEG based particles. Isotherms are expressed as percentage of the weight uptake with the dry mass taken as reference. Inserts show a magnification of isotherms at low %RH and water uptake kinetics.

Figure 10: Micromeritic and aerodynamic properties of sCT loaded particles made of PVP and L-PEG or B-PEG. Particles were formulated by spray drying solutions containing 1 wt% of PEG – PVP polymers present in a 1/1 (w/w) proportion and composed of acetone/water in a 7/3 weight ratio. A) Volume median diameters of the particle size distribution determined by laser diffraction B) Mass median aerodynamic diameter C) Geometric standard deviation of the aerodynamic particle size distribution D) Fine particle fraction expressed as percentage of the recovered particles. Data are the average of 3 measurements. ** ($P < 0.01$), * ($P < 0.05$). (ND: Not determined).

Figure 11: Percentage of cAMP in T47D cells versus sCT concentration for the unprocessed sCT and for the L-PEG and B-PEG-based formulations. Data are expressed as a percentage of the higher cAMP concentration obtained with the unprocessed sCT. Data are the average of 3 measurements. * ($P < 0.05$).

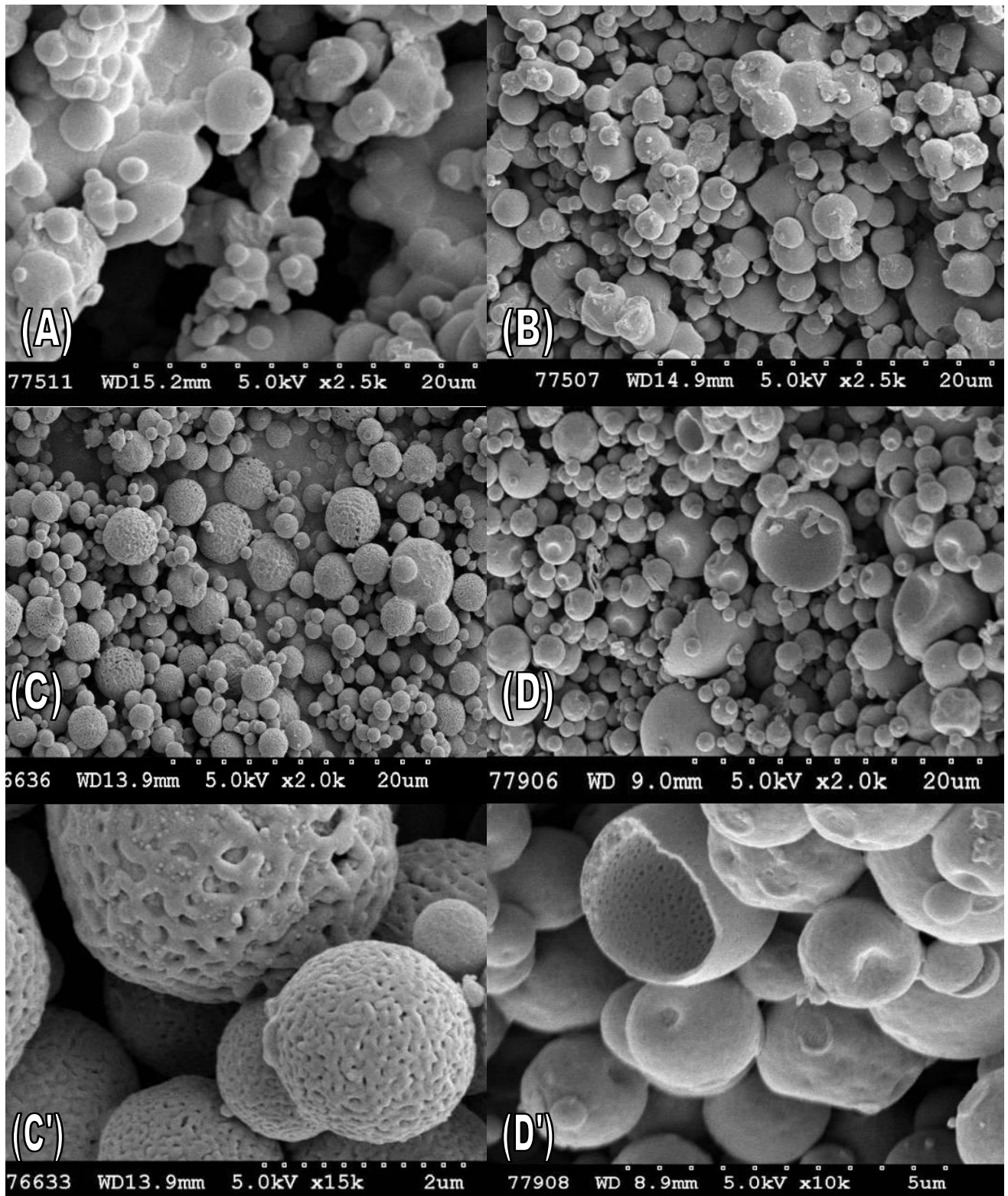


Figure1

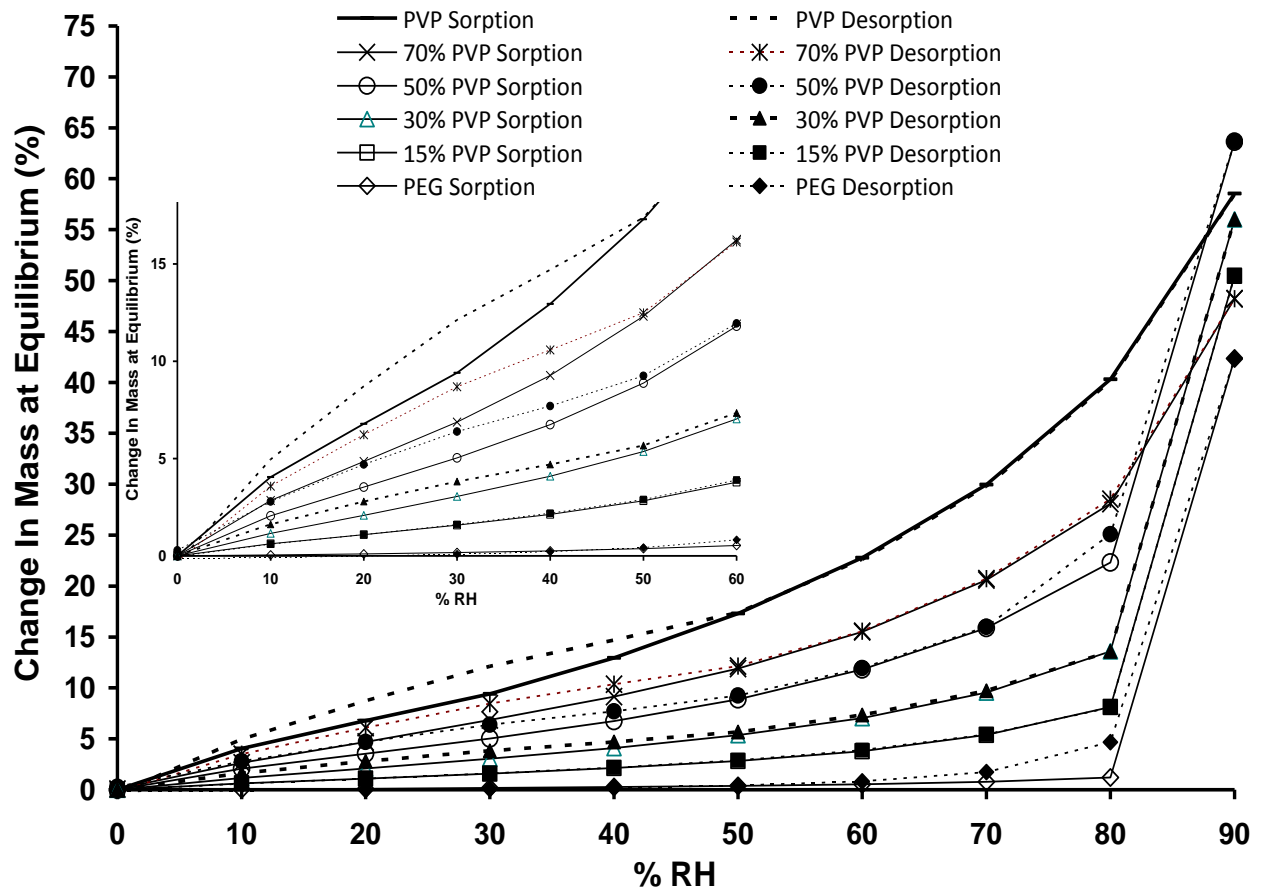


Figure 2.

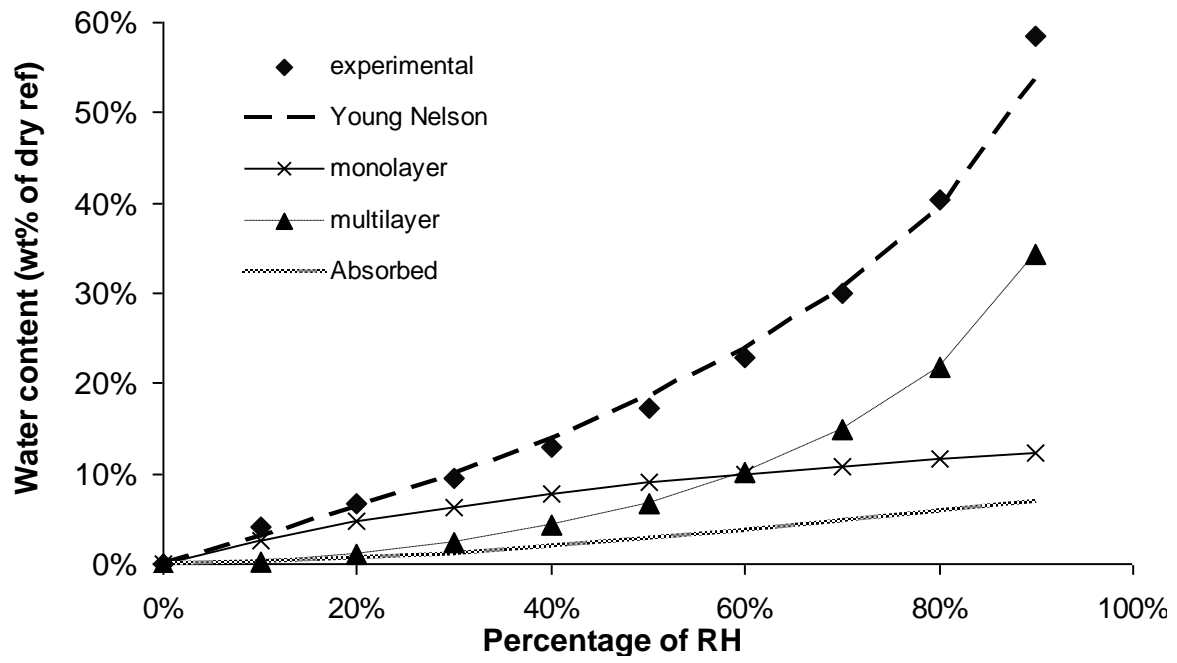


Figure 3.

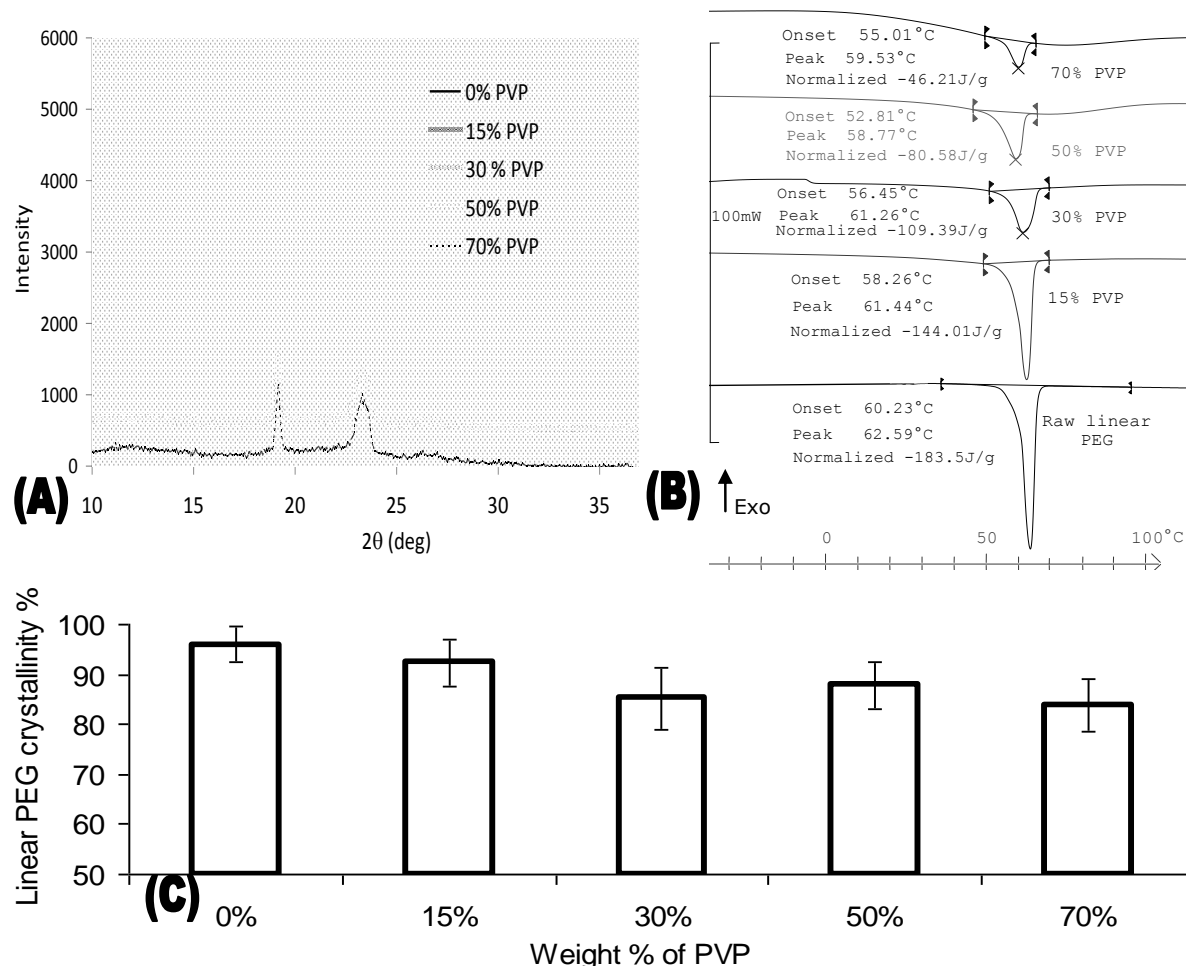


Figure 4.

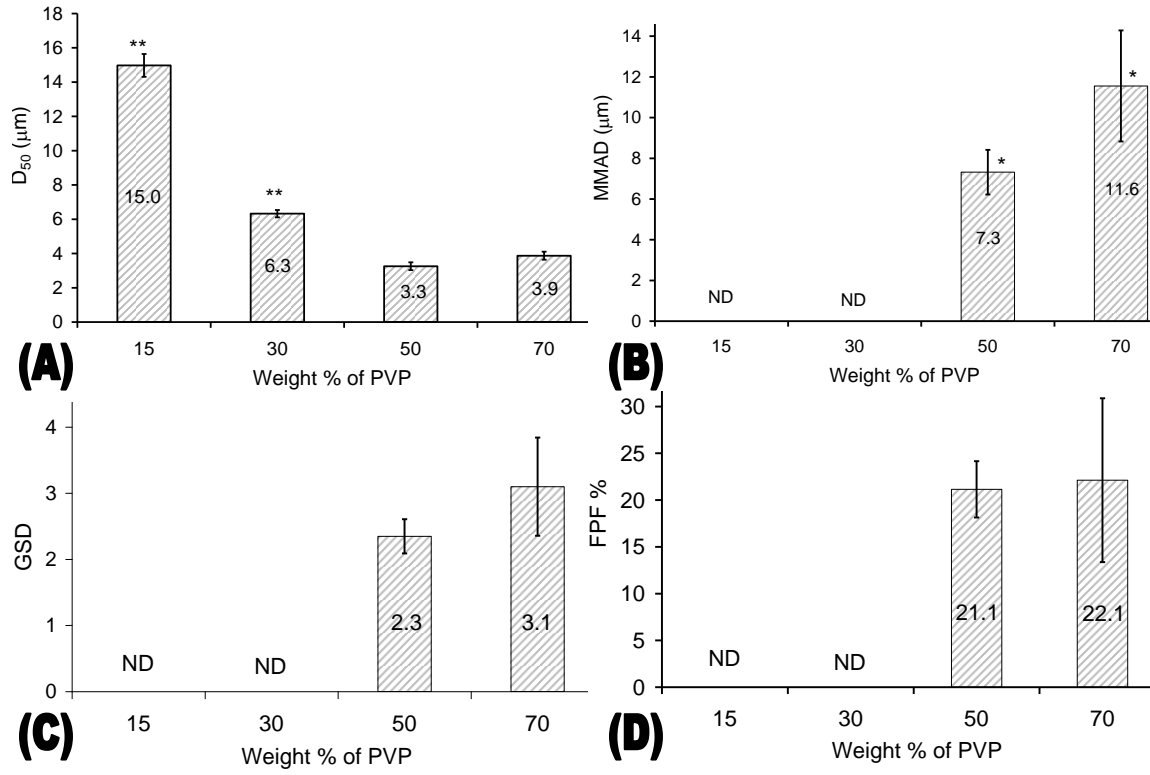


Figure 5.

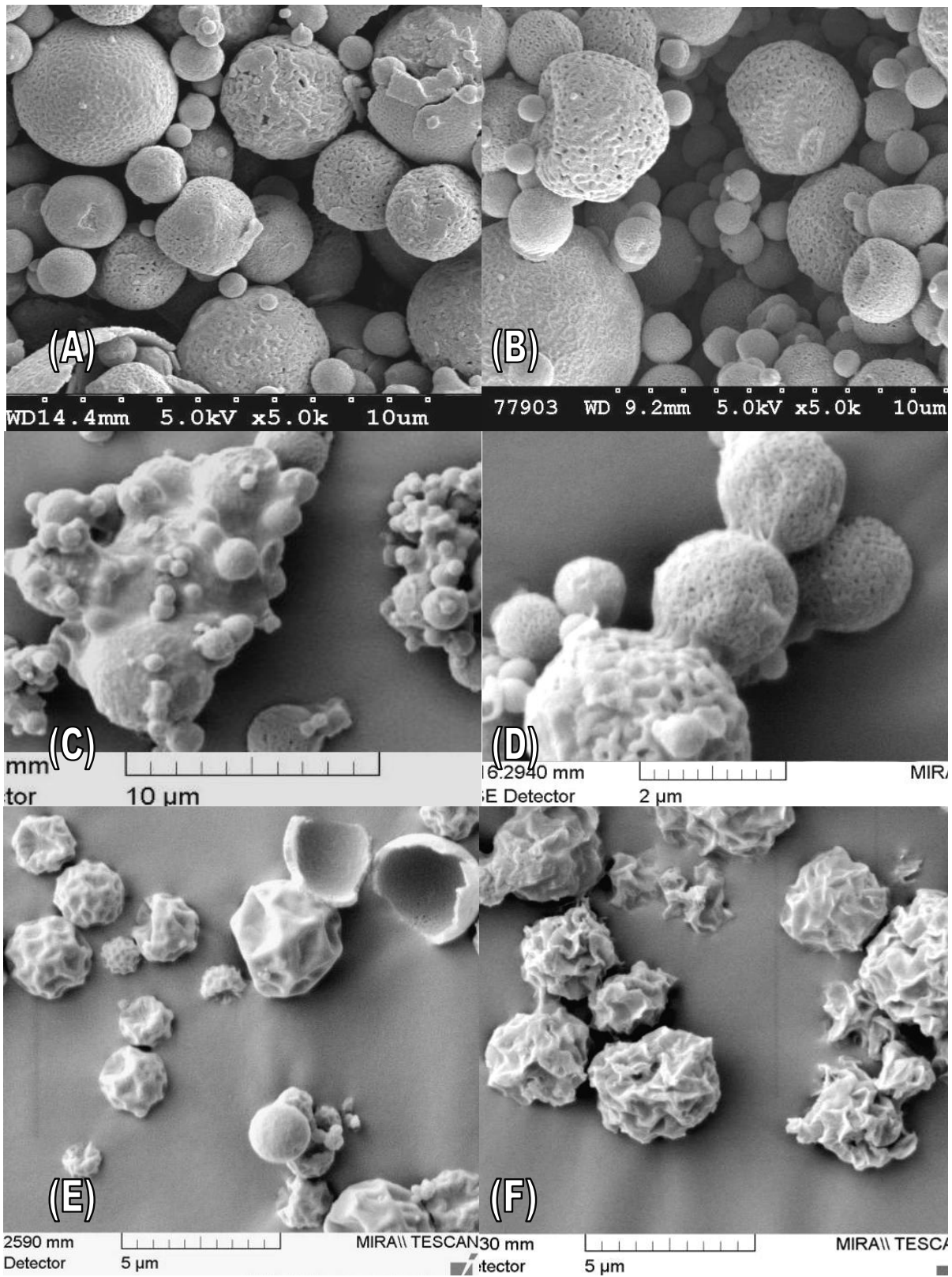


Figure 6

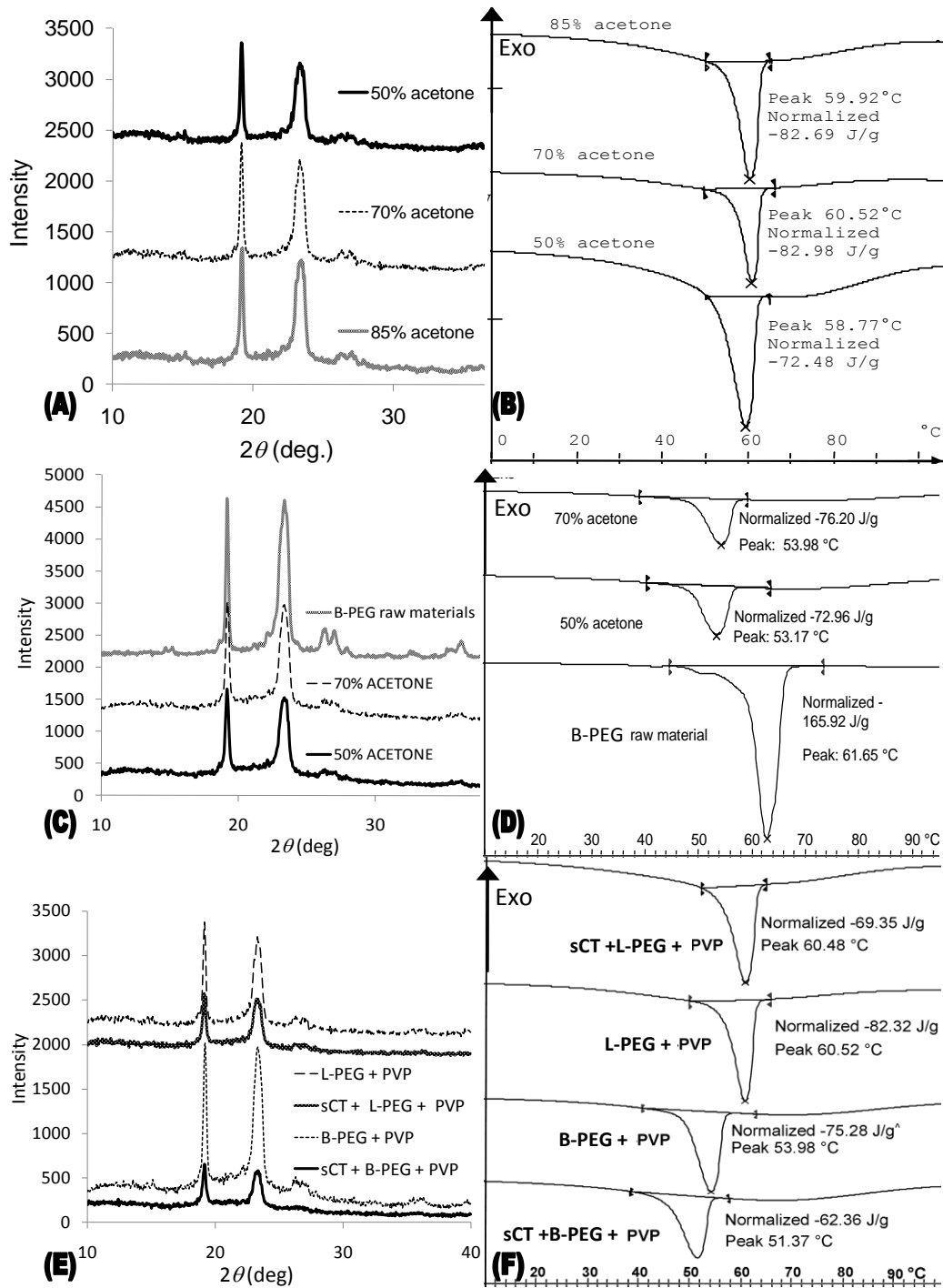


Figure 7

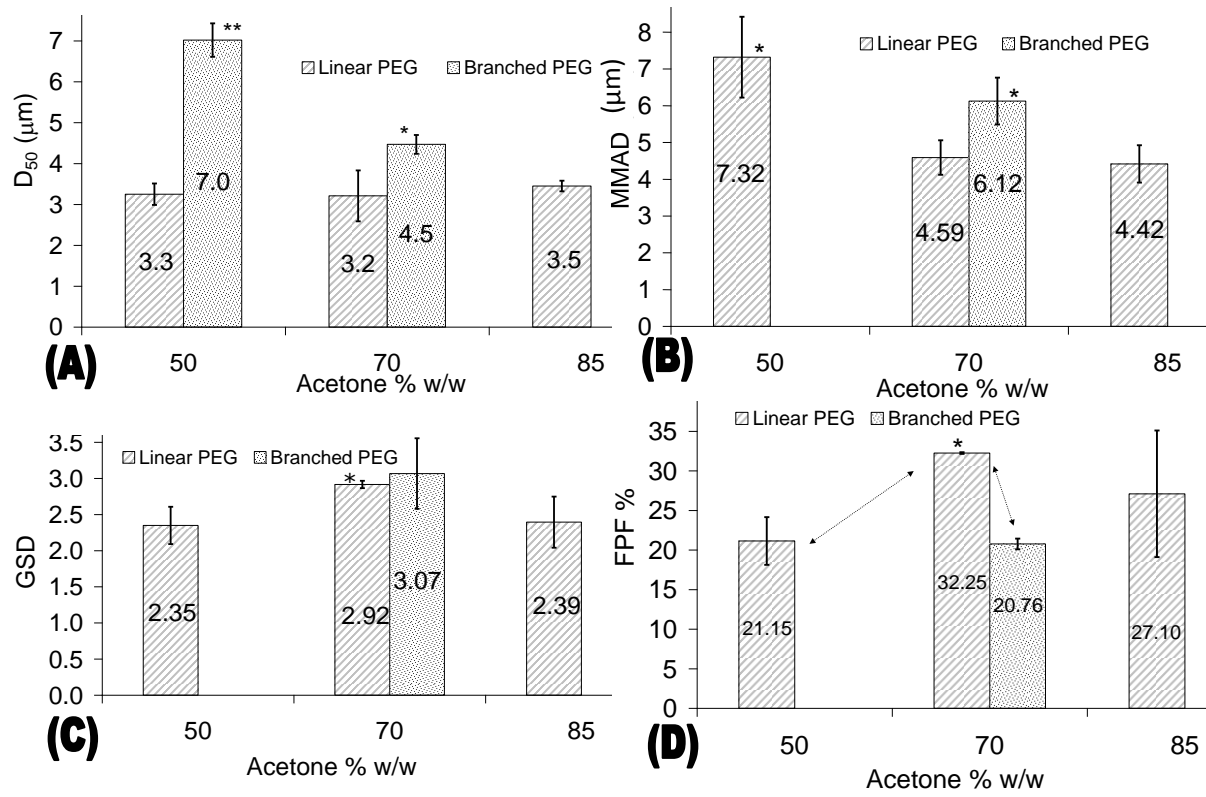


Figure 8

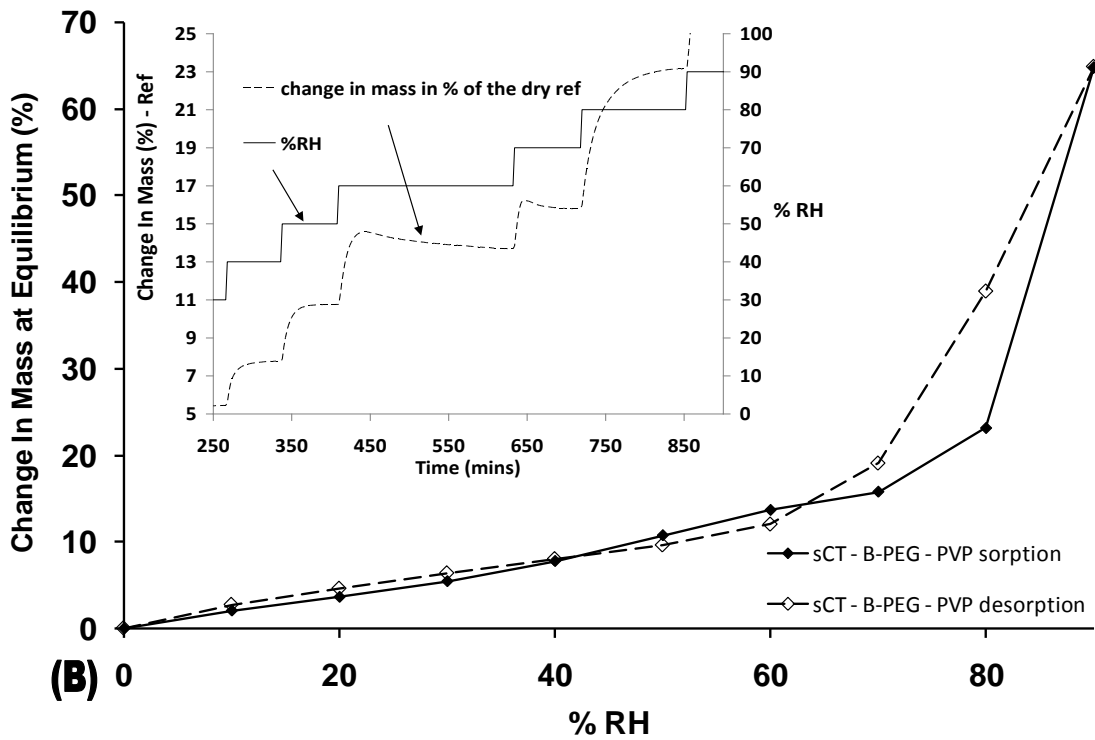
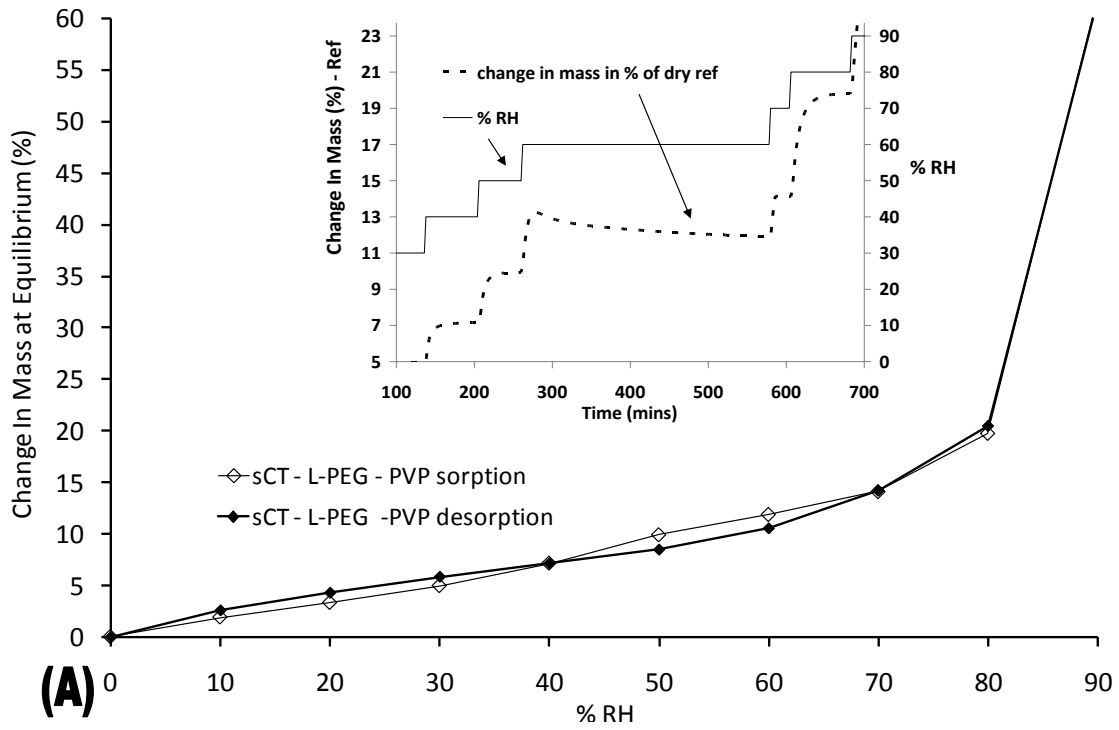


Figure 9

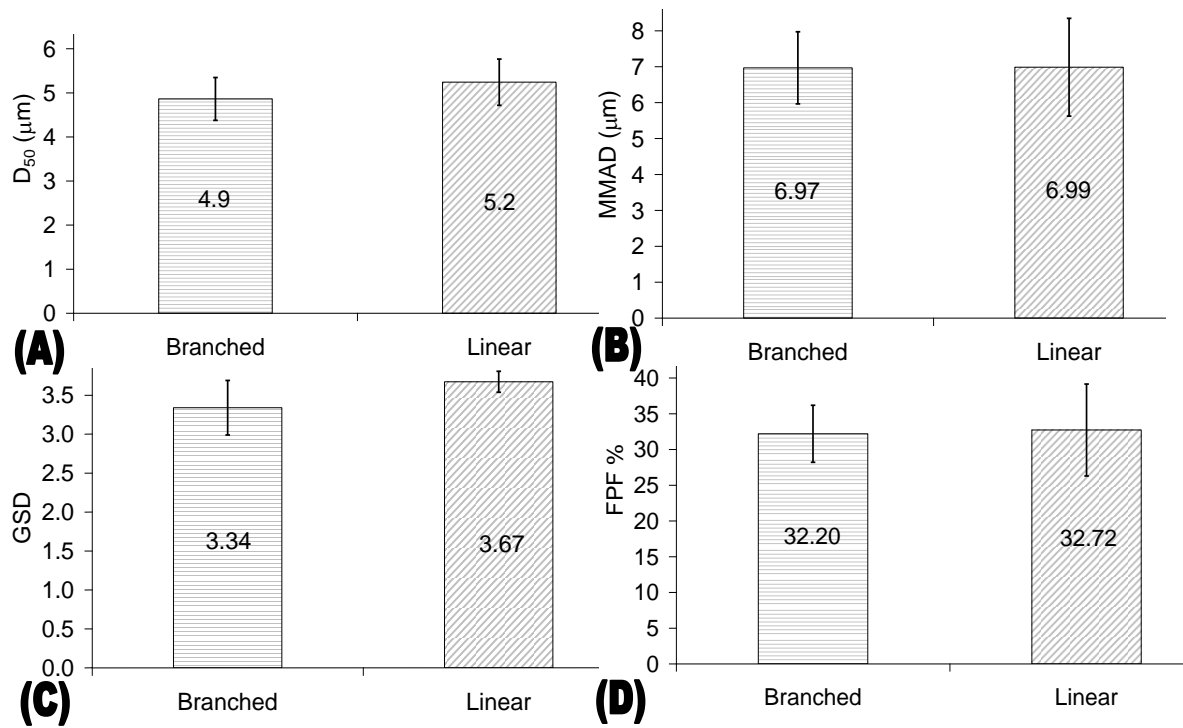


Figure 10.

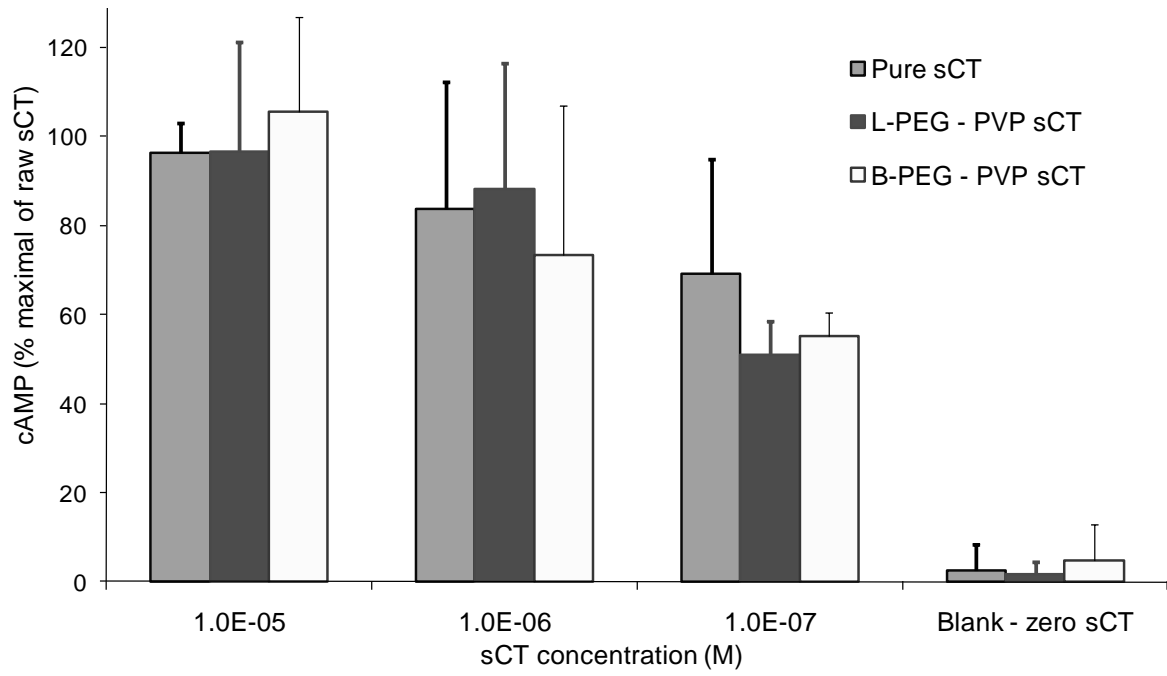
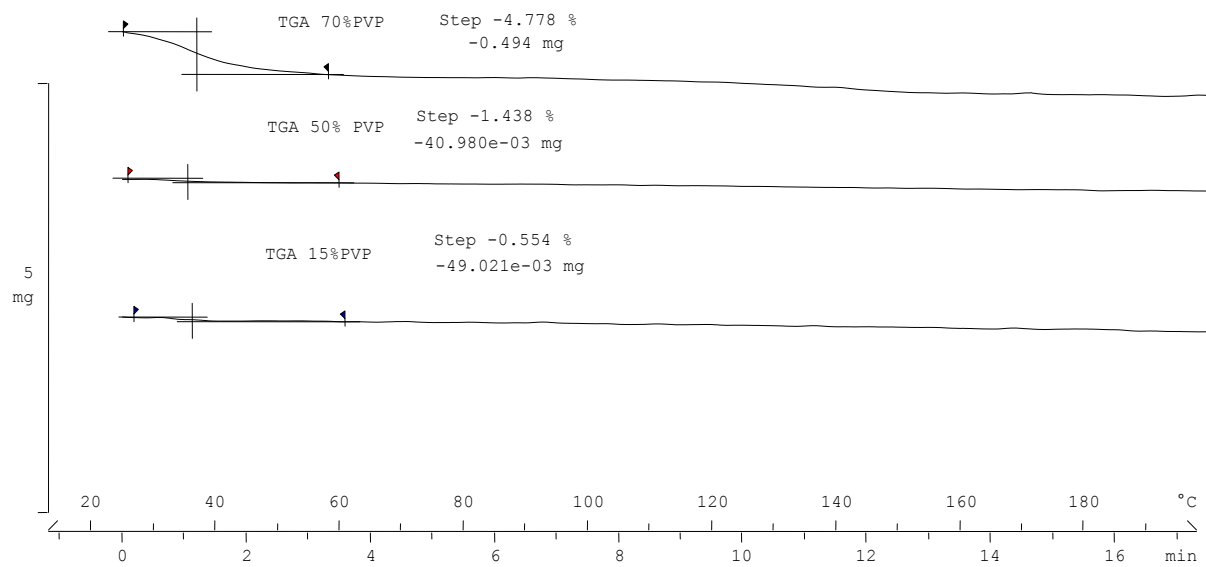


Figure 11



Additional information: TGA curves obtained for L-PEG – PVP particles composed of various amount of PVP (15 – 70 wt%)